2005-06-27

A PAM Decomposition of Weak CPM

Mason B. Wardle
Brigham Young University - Provo

A PAM DECOMPOSITION OF WEAK CPM

by

Mason B. Wardle

A thesis submitted to the faculty of

Brigham Young University

in partial fulfillment of the requirements for the degree of

Master of Science

Department of Electrical and Computer Engineering

Brigham Young University

August 2005

BRIGHAM YOUNG UNIVERSITY

GRADUATE COMMITTEE APPROVAL

of a thesis submitted by

Mason B. Wardle

This thesis has been read by each member of the following graduate committee and by majority vote has been found to be satisfactory.

Date	Michael D. Rice, Chair
Date	Michael A. Jensen
Date	A. Lee Swindlehurst

BRIGHAM YOUNG UNIVERSITY

As chair of the candidate's graduate committee, I have read the thesis of Mason B. Wardle in its final form and have found that (1) its format, citations, and bibliographical style are consistent and acceptable and fulfill university and department style requirements; (2) its illustrative materials including figures, tables, and charts are in place; and (3) the final manuscript is satisfactory to the graduate committee and is ready for submission to the university library.

Date

Michael D. Rice
Chair, Graduate Committee

Accepted for the Department

Michael A. Jensen
Graduate Coordinator

Accepted for the College

Alan R. Parkinson
Dean, Ira A. Fulton College of
Engineering and Technology

ABSTRACT

A PAM DECOMPOSITION OF WEAK CPM

Mason B. Wardle

Department of Electrical and Computer Engineering

Master of Science

The Enhanced Flight Termination System uses weak CPM as its modulation scheme and a limiter-discriminator as its demodulation scheme. A PAM representation of weak CPM was developed which representation provided the necessary componenents to build a simplified PAM-based receiver that outperformed the EFTS limiter-discriminator, even in the presence of phase noise. The PAM representation also provided a new perspective into the negative characteristics of weak CPM.

ACKNOWLEDGMENTS

I would like to acknowledge first and foremost my Heavenly Father Who constantly provided me with motivation and energy to complete this work. He also gave me a small yet crucial burst of inspiration that sent me in the right direction to develop a PAM representation for weak CPM.

Next, I would like to thank my wife for her love and support, who gave me motivation to work hard. She helped me continue when I was depressed and felt I could not continue. She has simply made my life better ever since she became a part of it.

I would also like to thank my family for their help in urging me to be a good student and to work hard to be succesful. My father deserves special thanks for my success as he helped me learn to work. My mother has also been there for me as I struggled my way through school.

Last but not least, I would like to mention the tremendous support I received while at BYU from the Electrical Engineering (EE) Department. First in this list is my professor and advisor, Professor Michael Rice, who so generously supported me, both financially and academically, as I pursued my master's degree. He also gave freely of his time to help me understand and make progress on my research as well as gave me the space and time I needed to ultimately make the findings I have.

I would also like to recognize the support of so many of the professors in the EE department as well as the terrific staff, including Ann Tanner. Their friendship and help was greatly appreciated. Also not to be neglected are the many friends who are studying in the Electrical Engineering department including the folks in the Telemetry Lab.

Contents

List of Tables

List of Figures

Chapter 1

Introduction

Most range safety programs use a Flight Termination System (FTS) to bring stray airborne test vehicles to crash at a preselected location, by bringing the vehicle into a state of zero lift and zero thrust. Methods used to meet this goal include parachute deployment and detonation of explosive charges that destroy the test vehicle [1]. The test range initiates flight termination by sending a radio signal on a dedicated channel to the stray test vehicle. The first FTS, brought into use in the 1950s, modulates a frequency modulation (FM) carrier with different frequency audio tones [2]-[4]. The aircraft completes the "arm" and "terminate" commands after the arrival of a predefined sequence of these tones from the ground-based transmitter [2]. The modified high-alphabet system [5] adds a security feature by using a predefined sequence of tone *pairs* to encode the commands.

With the increase in flight altitudes came an incident where the terminate signal sent by one test range inadvertently terminated the flight of a vehicle at a nearby test range [1, 6]. In response to this incident, the Range Safety Group of the Range Commanders Council created a committee in April 2000 to enumerate the requirements of the next generation FTS that would search for techniques to deal with the aforementioned situation. In January 2002, this group chose bi-phase pulse-coded modulation/frequency modulation (PCM/FM) as the modulation for the next generation FTS, named Enhanced Flight Termination System (EFTS) [7]. The justification behind this choice of modulation included the important reason that the ground-based FTS transmitter (i.e., the current hardware infrastructure) required an AC-coupled input to the FM modulator [8]. The EFTS standard chose a more "digital" route for the EFTS waveform which opened the door for better security (3DES encryption) and a higher level of reliability (Reed-Solomon error control coding).

The selection of bi-phase (also known as Manchester) PCM/FM (also known as continuous-phase modulation or CPM) included the assumption that the airborne vehicle would use a FM limiter-discriminator for a demodulator because the FM limiter-discriminator has a history of reliability in aeronautical applications. Unfortunately, this FM limiter-discriminator detector, (i.e., a simple FM-demodulator followed by a comparator) has a much poorer bit-error rate (BER) than an optimal receiver. An optimum receiver, on the other hand, requires a maximum-likelihood sequence detector and full phase coherency which is difficult to attain in the presence of excessive amounts of phase noise resulting from the high levels of shock and vibration typical in airborne vehicles.

In spite of this difficulty, consider such an optimum receiver. One method for designing an optimal receiver utilizes the Viterbi algorithm to effect maximum likelihood sequence estimation (MLSE). This approach yields a much lower BER at the expense of increased complexity, which comprises part of the difficulty of taking an optimal approach in EFTS. Anderson, Aulin, and Sundberg suggested a handful of techniques that facilitate the construction of simplified receivers for CPM which receivers have sub-optimal performance [9, chapter 8]; however, they can perform better than an FM limiter-discriminator. Pierre Laurent also presented a method for simplified receiver design. He showed that CPM can be reformulated as a sum of several PAM pulses [10]. (His results were later extended to M-ary CPM by Mengali [11][1] and to multi-h CPM by Perrins and Rice [13].) Using all of the pulses leads to MLSE detection; using fewer pulses results in a simplified receiver, but still with better expected performance than an FM demodulator.

The design of a simplified PAM receiver for EFTS-based CPM that outperforms, and maintains roughly the same level of complexity of, the current EFTS receiver would be possible;[2] this design goal motivated my research. Before diving into an explanation of my research, a review of CPM and its PAM representation will be presented.

[1] Mengali also developed a method to form a PAM representation of CPM when the modulation index is an integer. Another approach to forming a PAM representation for an integer modulation index can be found in [12]

[2] This assumes that full phase coherency is achievable in the presence of such severe phase noise as that found in EFTS applications

1.1 Definition of CPM

The complex-envelope of the transmitted CPM signal, $s(t)$, is defined as

$$s(t) = \exp\left(j2\pi h \int_{\tau=-\infty}^{t} \sum_{n=-\infty}^{N} \alpha(n) f(\tau - nT)\, d\tau\right) \tag{1.1}$$

where $f(t)$ is termed the frequency pulse and has a region of support (spans an interval of time) typically restricted to $0 < t < LT$ where T is the symbol time and L is the number of symbol times spanned by the frequency pulse. Also, $\alpha(n)$ represents the n-th binary data symbol and the modulation index, h, which dictates how much the phase changes for each symbol. (Note that the frequency pulse dictates how the frequency of the complex exponential changes as a function of time.) Reversing the order of the integral and the summation in (1.1) and performing integration yields

$$s(t) = \exp(j \cdot 2\pi h \cdot \phi(t)) \tag{1.2}$$

where

$$\phi(t) = \sum_{n=-\infty}^{N} \alpha(n) g(t - nT) \quad t \leq (N+1)T \tag{1.3}$$

$$g(t) = \int_{-\infty}^{t} f(\tau)\, d\tau. \tag{1.4}$$

Three design parameters available in CPM are the choice of the frequency pulse and the choice of the symbol alphabet. The modulation index, h, is set depending on the application. Henceforth, the alphabet will be assumed to be binary. The choice of frequency pulse (or phase pulse, depending on the perspective), can dramatically affect the behavior of the CPM signal. The phase pulseis most often defined as:

$$g(t) = \begin{cases} 0 & t \leq 0 \\ \frac{1}{2} & t \geq LT \end{cases} \tag{1.5}$$

which implies that the phase pulse has an infinite length, although it is constant for $t > LT$.

Weak CPM In rare cases, the frequency pulse is defined such that the phase pulse has a finite length (EFTS being one such case). Looking at (1.4) and (1.5), one can see that the

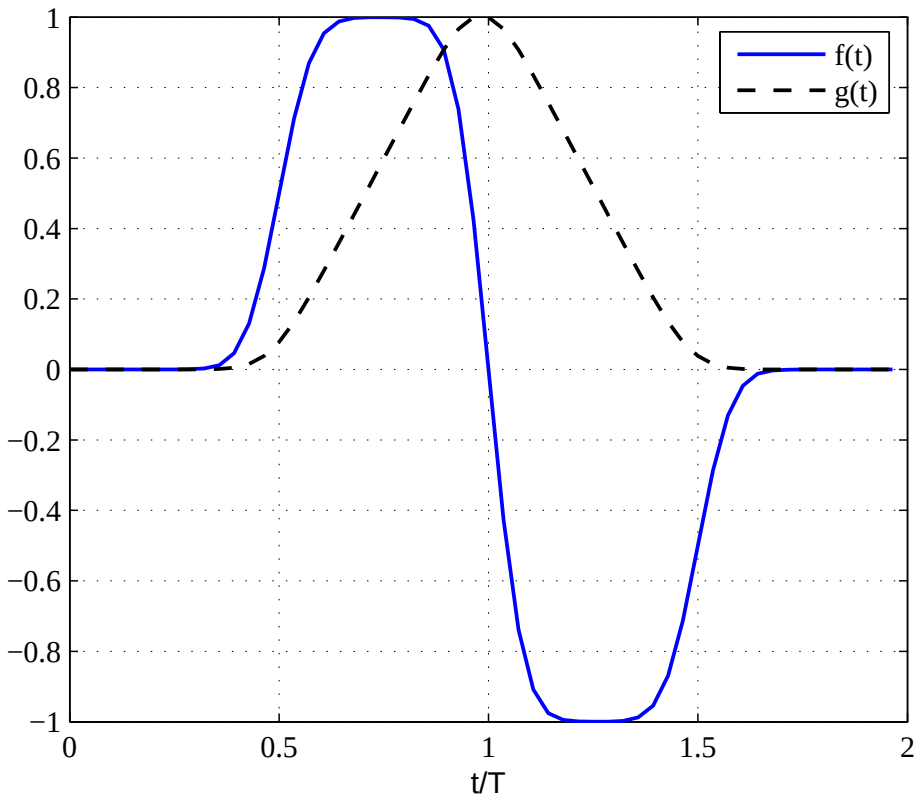

Figure 1.1: The frequency and phase pulses for the EFTS weak CPM. (Note: the pulses have been normalized to unit peak amplitude for display.)

frequency pulse must integrate to zero in such a case. The phase pulse is thus defined for this case as

$$g(t) = 0 \qquad t \leq 0 \text{ and } t \geq LT. \tag{1.6}$$

Figure 1.1 presents the plot of one example of such a frequency-pulse/phase-pulse pair. A frequency pulse of this type has been termed *weak* [9, page 64]. Thus, from this point forward, CPM based on such a frequency pulse will be termed *weak* CPM, whereas CPM based on the more common frequency pulse, whose phase pulse is defined in (1.5), will simply be termed *CPM*. The reason behind naming the frequency pulse weak comes from the effect a weak frequency pulse has on the frequency spectrum and on the minimum Euclidean distance of the CPM signal; these effects will be investigated in Sections 2.4 and 3.1, respectively. References [14]-[22] present some of the limited research completed for weak CPM.

1.2 PAM Decomposition of CPM

The PAM representation presented by Laurent facilitates the design of simplified receivers since there has been extensive research performed on linear[3] modulations (modulations which include PAM); examples of this research include synchronization methods and optimal receivers [23].

1.2.1 Exact Representation

Laurent showed that a binary CPM signal, $s(t)$, can be reformulated as

$$s(t) = \sum_{N=-\infty}^{\infty} \sum_{K=0}^{2^{L-1}-1} a_K(N) C_K(t - NT) \tag{1.7}$$

where

$$C_K(t) = \prod_{i=0}^{L-1} u(t + [i + \beta_K(i)L]T) \tag{1.8}$$

$$u(t) = \frac{\sin[\Psi(t)]}{\sin(\pi h)} \tag{1.9}$$

$$\Psi(t) = \begin{cases} 2\pi h g(t) & t < LT \\ \pi h - 2\pi h g(t - LT) & t \geq LT \end{cases} \tag{1.10}$$

$$a_K(N) = J^{A_K(N)} \tag{1.11}$$

$$A_K(N) = \sum_{n=-\infty}^{N} \alpha(n) - \sum_{i=1}^{L-1} \alpha(N-i) \cdot \beta_K(i) \tag{1.12}$$

$$K = \sum_{i=1}^{L-1} 2^{i-1} \cdot \beta_K(i) \quad 0 \leq K \leq 2^{L-1} - 1 \tag{1.13}$$

$$J = e^{j\pi h} \tag{1.14}$$

and $\beta_K(i)$ is the i-th coefficient for the radix-2 decomposition of an integer K. (Appendix A presents a complete derivation of this PAM decomposition.) Equation (1.7) contains a sum of PAM pulses for each N. In Laurent's derivation, the sums of PAM pulses are divided into

[3]PAM representations of CPM transform the non-linear CPM into a linear PAM modulation by pushing the non-linearity out of the modulation into the data symbols. The most important reason for making this representation is that it allows the design of a demodulator to perform sub-optimal detection as explained later.

groups. Each group consists of all PAM pulses that start in the interval $NT < t < (N+1)T$ for a given value of N. This grouping becomes useful in understanding the derivation of the PAM representation in Chapter 2.

1.2.2 Approximate Representation

Generally speaking, in a PAM decomposition, one pulse or perhaps a few pulses comprise most of the energy in the CPM signal. The use of only the most energetic PAM pulses provides a receiver with acceptable performance. This ease of approximation helps the PAM representation finds its niche: the PAM representation opens up a path to build a simplified receiver. (See reference [24].) The approximation gives a simple way to reduce complexity, while limiting the inevitable increase in BER relative to that of an optimal receiver. Simualtion results presented in Chapter 3 showed that a simplified PAM-based receiver greatly outperforms an FM demodulator.

1.2.3 PAM Representation of Weak CPM

In order to build a simplified receiver, a PAM representation of weak CPM, which was not provided by Laurent, must be developed; my research has focused on such a development. Weak CPM is shown to have a PAM representation, just as CPM does. Such a representation provided a new perspective to the failings of weak CPM. Most importantly, this PAM representation gave a way to build a simplified EFTS receiver by following the work of Ghassan Kaleh [24]; this simplified receiver performed significantly better than an FM limiter-discriminator, even in the presence of phase noise that arises in EFTS applications.

Chapter 2 derives a PAM representation for weak CPM. Chapter 3 shows how to build weak CPM receivers and presents simulation results for EFTS PAM-based receivers.

Chapter 2

Weak CPM PAM Signal Representation

Laurent's 1986 paper did not consider the rarely used weak CPM. The whole idea of Laurent's work aimed to find a linear PAM decomposition, but Laurent's method applied directly to weak CPM yields a non-linear PAM decomposition. However, my work has derived a linear PAM representation for weak CPM using an approach to Laurent's work similar to that taken by Mengali and Morelli to create a PAM representation for M-ary CPM [11].

Section 2.1 demonstrates the need for an approach different than that of Laurent's. Section 2.2 derives the PAM representation of weak CPM; the end of this section presents a summary of an approach to calculate a general PAM representation for weak CPM Finally, Section 2.3 finds the PAM pulses for EFTS-based CPM, and Section 2.4 shows how discrete lines surface in the spectrum of weak CPM.

2.1 The Need For a New Approach

A comparison of Laurent PAM decompositions of CPM and weak CPM demonstrates the need for a new approach in formulating a PAM representation of weak CPM. An extended example (used throughout this chapter) illustrates this need in a straightforward way as well as logically develops a new approach.

Example for L=2 Part 1

Appendix A shows that

$$\exp\big[j\pi h\alpha(n)g(t-nT)\big] = u\big(t+[L-n]T\big) + J^{\alpha(n)}u(t-nT), \tag{2.1}$$

with $u(t)$ defined in (1.9). Equation (2.1) allows $s(t)$, the CPM signal, to be expressed by the following equation:

$$s(t) = J^{\sum_{n=-\infty}^{(N-L)} \alpha(n)} \prod_{i=0}^{L-1} \Big[u\big(t + [i + L - N]T\big) + J^{\alpha(N-i)} u\big(t + [i - N]T\big) \Big]. \tag{2.2}$$

(For a full derivation, consult Appendix A). Using the time interval $NT < t < (N+1)T$ for $N = 0, 1, 2$ and $L = 2$, equation (2.2) becomes:

$$\begin{aligned}
0 < t < T: \quad s(t) &= J^{\sum_{n=-\infty}^{-2} \alpha(n)} \cdot \big[C_0(t + 2T) \\
&\quad + J^{\alpha(-1)} C_0(t + T) + J^{\alpha(0)+\alpha(-1)} C_0(t) + J^{\alpha(0)} C_1(t) \big] \\
T < t < 2T: \quad s(t) &= J^{\sum_{n=-\infty}^{-2} \alpha(n)} \cdot \big[J^{\alpha(-1)} C_0(t + T) \\
&\quad + J^{\alpha(0)+\alpha(-1)} C_0(t) + J^{\alpha(1)+\alpha(0)+\alpha(-1)} C_0(t - T) \\
&\quad + J^{\alpha(1)+\alpha_(-1)} C_1(t - T) \big] \\
2T < t < 3T: \quad s(t) &= J^{\sum_{n=-\infty}^{-2} \alpha(n)} \cdot \big[J^{\alpha(0)+\alpha(-1)} C_0(t) \\
&\quad + J^{\alpha(1)+\alpha(0)+\alpha(-1)} C_0(t - T) + J^{\alpha(2)+\alpha(1)+\alpha(0)+\alpha(-1)} C_0(t - 2T) \\
&\quad + J^{\alpha(2)+\alpha(0)+\alpha(-1)} C_1(t - 2T) \big].
\end{aligned} \tag{2.3}$$

The coefficents of shifted versions of C_K terms for a given value of K are all the same. For example, the coefficient for $C_0(t)$ is $J^{\alpha(0)+\alpha(-1)}$ for $0 < t < 3T$ and the coefficient for $C_0(t + T)$ is $J^{\alpha(-1)}$ for $0 < t < 2T$. $\big(C_0(t + T)$ is zero for $t > 2T.\big)$ This characteristic ultimately allows the reformation of CPM into linear PAM. This reformation, found in (1.7) and repeated here for convenience, expands (2.3) to include all N:

$$s(t) = \sum_{N=-\infty}^{\infty} \sum_{K=0}^{2^{L-1}-1} a_K(N) C_K(t - NT) \tag{2.4}$$

$$\text{where} \quad C_K(t) = \prod_{i=0}^{L-1} u\big(t + [i + \beta_K(i)L]T\big) \tag{2.5}$$

$$u(t) = \frac{\sin\big[\Psi(t)\big]}{\sin(\pi h)} \tag{2.6}$$

$$\Psi(t) = \begin{cases} 2\pi h g(t) & t < LT \\ \pi h - 2\pi h g(t - LT) & t \geq LT \end{cases} \tag{2.7}$$

$$a_K(N) = J^{A_K(N)} \tag{2.8}$$

$$A_K(N) = \sum_{n=-\infty}^{N} \alpha(n) - \sum_{i=1}^{L-1} \alpha(N-i) \cdot \beta_K(i) \tag{2.9}$$

$$K = \sum_{i=1}^{L-1} 2^{i-1} \cdot \beta_K(i) \quad 0 \leq K \leq 2^{L-1} - 1 \tag{2.10}$$

$$J = e^{j\pi h}. \tag{2.11}$$

On the other hand, applying weak CPM to (2.2) for $N = 0, 1, 2$ yields:

$$\begin{aligned}
0 < t < T: \quad s(t) &= \big[C_0(t+2T) + J^{\alpha(-1)} C_0(t+T) + J^{\alpha(0)+\alpha(-1)} C_0(t) \\
&\quad + J^{\alpha(0)} C_1(t)\big] \\
T < t < 2T: \quad s(t) &= \big[C_0(t+T) + J^{\alpha(0)} C_0(t) + J^{\alpha(1)+\alpha(0)} C_0(t-T) \\
&\quad + J^{\alpha(1)} C_1(t-T)\big] \\
2T < t < 3T: \quad s(t) &= \big[C_0(t) + J^{\alpha(1)} C_0(t-T) + J^{\alpha(2)+\alpha(1)} C_0(t-2T) \\
&\quad + J^{\alpha(2)} C_1(t-2T)\big].
\end{aligned} \tag{2.12}$$

Now in this case, unlike generic CPM shown in (2.3), the coefficients of the C_K terms change with each N. For example, consider again $C_0(t)$. For $0 < t < T$, $C_0(t)$ has a coefficient of $J^{\alpha(0)+\alpha(-1)}$; for $T < t < 2T$, this coefficient becomes $J^{\alpha(0)}$. This makes it impossible, using this form, to create a linear PAM expression for $s(t)$ for all t. Thus, Laurent's PAM approach applied to weak CPM does not yield a linear result, and so another approach must be taken to find a linear PAM representation of weak CPM.

2.2 General PAM Decomposition of Weak CPM

In order to derive a PAM decomposition for weak CPM, the signal will be split into the product of two different CPM signals. This method of rewriting CPM as the product of two CPM signals can also be found in [11].

2.2.1 Derivation of PAM Representation

Consider a frequency pulse, $f(t)$, of length LT, that integrates to zero. In calculating the PAM decomposition for CPM based on this frequency pulse, the first step is to

divide the frequency pulse into two pulses:

$$f(t) = f^+(t) + f^-(t) \tag{2.13}$$

where

$$\begin{aligned} f^+(t) &= \begin{cases} f(t) & f(t) > 0 \\ 0 & \text{otherwise} \end{cases} \\ f^-(t) &= \begin{cases} f(t) & f(t) < 0 \\ 0 & \text{otherwise} \end{cases} . \end{aligned} \tag{2.14}$$

The next step is to calculate the phase pulses $g^+(t)$ and $g^-(t)$, which are equal to the integral of $f^+(t)$ and the integral of $f^-(t)$, respectively. Thus $g(t)$, which is the integral of $f(t)$, as defined in (1.4), can be expressed as the sum of two shorter-length phase pulses:

$$g(t) = g^+(t) + g^-(t). \tag{2.15}$$

Clearly, if $g^+(LT) = 1/2$, then $g^-(LT) = -1/2$, since for weak CPM, $g(LT) = 0$. The PAM representation of $g^+(t)$ can be formulated using (2.4) and assuming $g^+(t)$ is the same length as $g(t)$.

With a slight modification to Laurent's original development, we can in a similar manner find the PAM representaion for $g^-(t)$. To find the PAM representaion for $g^-(t)$, note that CPM based on a frequency pulse that integrates to $-1/2$ is just like CPM with a frequency pulse that integrates to A but has each α_i negated. Making this modification to (2.9), (2.4) becomes

$$s^-(t) = \sum_{N=-\infty}^{\infty} \sum_{K=0}^{2^{L-1}-1} a_K^*(N) D_K(t - nT) \tag{2.16}$$

where * denotes complex-conjugation and the D_K's are the PAM pulses for $-g^-(t)$. (For a derivation of this modification see Appendix A.)

Recalling (1.2) and using $f(t)$ as defined in (2.14), $s(t)$ can now be rewritten as

$$s(t) = \exp\ j[\sum_{n=-\infty}^{\infty} \alpha(n) g^+(t - nT)] \cdot \exp\ j[\sum_{n=-\infty}^{\infty} \alpha(n) g^-(t - nT)]. \tag{2.17}$$

Applying Laurent's PAM decomposition to both terms in this product yields

$$s(t) = \sum_{N=-\infty}^{\infty} \sum_{K=0}^{2^{L-1}-1} a_K(N) C_K(t - NT) \cdot \sum_{N'=-\infty}^{\infty} \sum_{K'=0}^{2^{L-1}-1} a^*_{K'}(N') D_{K'}(t - N'T). \quad (2.18)$$

Example for $L = 2$ Part 2

Consider an expansion of the product of sums in (2.18), where the group of PAM pulses that are nonzero in the interval $0 < t < T$ will be considered. Thus (2.18) for $0 < t < T$ is:

$$\begin{aligned}
s(t) = {} & a_0(0) \cdot a_0^*(0) C_0(t) D_0(t) \\
& + a_0(0) \cdot a_1^*(0) C_0(t) D_1(t) \\
& + a_0(0) \cdot a_0^*(-1) C_0(t) D_0(t+T) \\
& + a_0(0) \cdot a_0^*(-2) C_0(t) D_0(t+2T) \\
& + a_1(0) \cdot a_0^*(0) C_1(t) D_0(t) \\
& + a_1(0) \cdot a_1^*(0) C_1(t) D_1(t) \\
& + a_1(0) \cdot a_0^*(-1) C_1(t) D_0(t+T) \\
& + a_1(0) \cdot a_0^*(-2) C_1(t) D_0(t+2T) \\
& + a_0(-1) \cdot a_0^*(0) C_0(t+T) D_0(t) \\
& + a_0(-1) \cdot a_1^*(0) C_0(t+T) D_1(t) \\
& \boldsymbol{+ a_0(-1) \cdot a_0^*(-1) C_0(t+T) D_0(t+T)} \\
& \boldsymbol{+ a_0(-1) \cdot a_0^*(-2) C_0(t+T) D_0(t+2T)} \\
& + a_0(-2) \cdot a_0^*(0) C_0(t+2T) D_0(t) \\
& + a_0(-2) \cdot a_1^*(0) C_0(t+T) D_1(t) \\
& \boldsymbol{+ a_0(-2) \cdot a_0^*(-1) C_0(t+2T) D_0(t+T)} \\
& \boldsymbol{+ a_0(-2) \cdot a_0^*(-2) C_0(t+2T) D_0(t+2T)} \, .
\end{aligned} \quad (2.19)$$

The terms of (2.19) in bold face are shifted versions of other pulses already present in (2.19). For example if $q_0(t) = C_0(t)D_0(t)$ and $d_0(0) = a_0(0)a_0^*(0)$, then $a_0(-2) \cdot a_0^*(-2)C_0(t + 2T)D_0(t + 2T) = d_0(-2)q_0(t + 2T)$. This term came into the picture in the time interval $-2T < t < -T$. Any pulse $q_i(t + NT)$, where its region of support began in the interval

$NT < t < (N+1)T\, N \neq 0$, will be removed from this group and placed in the group of pulses that also started in the interval $NT < t < (N+1)T\, N \neq 0$. Thus the terms in bold face belong in different groups; the first three belong in the group of pulses that start in the interval $-T < t < 0$ and the fourth pulse belongs with pulses that start in the interval $-2T < t < T$. (Laurent also regrouped the PAM pulses along the same lines; see Section 1.2.1 for further explanation.) Thus neglecting these terms, $s(t)$ for the group of PAM pulses for the interval $0 < t < T$ can be written as:

$$\begin{aligned} s(t) = {} & a_0(0) \cdot a_0^*(0) C_0(t) D_0(t) \\ & + a_0(0) \cdot a_1^*(0) C_0(t) D_1(t) \\ & + a_0(0) \cdot a_0^*(-1) C_0(t) D_0(t+T) \\ & + a_0(0) \cdot a_0^*(-2) C_0(t) D_0(t+2T) \\ & + a_1(0) \cdot a_0^*(0) C_1(t) D_0(t) \\ & + a_1(0) \cdot a_1^*(0) C_1(t) D_1(t) \\ & + a_1(0) \cdot a_0^*(-1) C_1(t) D_0(t+T) \\ & + a_1(0) \cdot a_0^*(-2) C_1(t) D_0(t+2T) \\ & + a_0(-1) \cdot a_0^*(0) C_0(t+T) D_0(t) \\ & + a_0(-1) \cdot a_1^*(0) C_0(t+T) D_1(t) \\ & + a_0(-2) \cdot a_0^*(0) C_0(t+2T) D_0(t) \\ & + a_0(-2) \cdot a_1^*(0) C_0(t+T) D_1(t). \end{aligned} \tag{2.20}$$

Thus, there are twelve unique PAM pulses in weak CPM with $L = 2$.

2.2.2 Simplifying the Exact Representation and Calculating the Number of PAM Pulses

At no point in the preceding derivation were approximations made. Therefore, (2.20) is an exact representation of weak CPM for $L = 2$, which equation can be simplified without deferring to an approximate representation.

Example for $L = 2$ Part 3

An examination of (2.20) shows that some of the pseudo-symbol products are equal. Since these products are coefficients of the PAM pulses, any products that are equal allow the combining of the PAM pulses corresponding to these products, thus reducing the number of PAM pulses without compromising the exact PAM representation in (2.20). This reduction will be performed using (2.8) which states that $a_K(N) = J^{A_K(N)}$; this means the simplification process will simply involve taking the difference between sums of various combinations of $\alpha(n)$. The pseudo-symbol products are:

$$a_0(0) \cdot a_0^*(0) = 1 \tag{2.21}$$

$$a_0(0) \cdot a_1^*(0) = J^{\alpha(-1)} \tag{2.22}$$

$$a_0(0) \cdot a_0^*(-1) = J^{\alpha(0)} \tag{2.23}$$

$$a_0(0) \cdot a_0^*(-2) = J^{\alpha(0)+\alpha(-1)} \tag{2.24}$$

$$a_1(0) \cdot a_0^*(0) = J^{-\alpha(-1)} \tag{2.25}$$

$$a_1(0) \cdot a_1^*(0) = 1 \tag{2.26}$$

$$a_1(0) \cdot a_0^*(-1) = J^{\alpha(0)-\alpha(-1)} \tag{2.27}$$

$$a_1(0) \cdot a_0^*(-2) = J^{\alpha(0)} \tag{2.28}$$

$$a_0(-1) \cdot a_0^*(0) = J^{-\alpha(0)} \tag{2.29}$$

$$a_0(-1) \cdot a_1^*(0) = J^{-\alpha(0)+\alpha(-1)} \tag{2.30}$$

$$a_0(-2) \cdot a_0^*(0) = J^{-\alpha(0)-\alpha(-1)} \tag{2.31}$$

$$a_0(-2) \cdot a_1^*(0) = J^{-\alpha(0)}. \tag{2.32}$$

Clearly

$$a_0(0) \cdot a_0^*(0) = a_1(0) \cdot a_1^*(0) \tag{2.33}$$

$$a_0(0) \cdot a_0^*(-1) = a_1(0) \cdot a_0^*(-2) \tag{2.34}$$

$$a_0(-1) \cdot a_0^*(0) = a_0(-2) \cdot a_1^*(0). \tag{2.35}$$

This results in the simplification of $s(t)$ for $0 < t < T$, where the newly combined pulses are displayed in bold face:

$$\begin{aligned} s(t) = & [\boldsymbol{C_0(t)D_0(t) + C_1(t)D_1(t)}] \\ & + J^{\alpha(-1)}C_0(t)D_1(t) \\ & + J^{\alpha(0)}[\boldsymbol{C_0(t)D_0(t+T) + C_1(t)D_0(t+2T)}] \\ & + J^{\alpha(0)+\alpha(-1)}C_0(t)D_0(t+2T) \\ & + J^{-\alpha(-1)}C_1(t)D_0(t) \\ & + J^{\alpha(0)-\alpha(-1)}C_1(t)D_0(t+T) \\ & + J^{-\alpha(0)}[\boldsymbol{C_0(t+T)D_0(t) + C_0(t+T)D_1(t)}] \\ & + J^{-\alpha(0)+\alpha(-1)}C_0(t+T)D_1(t) \\ & + J^{-\alpha(0)-\alpha(-1)}C_0(t+2T)D_0(t). \end{aligned} \tag{2.36}$$

Maximum Number of PAM Pulses Just as done in transforming (2.3) into (2.4), (2.36) can be generalized to include all time as follows:

$$s(t) = \sum_{N=-\infty}^{\infty} \sum_{K=0}^{P-1} d_K(N) q_K(t - NT) \tag{2.37}$$

where $P = 3^2$, $d_K(N)$ represents the new pseudo-symbols, and $q_K(t)$ is defined as the products of $C_K(t)$ and $D_K(t)$, each shifted by various amounts. As an example of $q_K(t)$, one might define the following:

$$\begin{aligned} q_0(t) &= C_0(t)D_0(t) + C_1(t)D_1(t) \\ q_1(t) &= C_0(t)D_1(t). \end{aligned} \tag{2.38}$$

(In actuality, $q_0(t)$ and $q_1(t)$ will be assigned different pulse-product combinations than those in (2.38); criteria for such assignment will be give later on.)

The pseudo-symbols in (2.36) are functions only of the current and previous data symbols and their coefficients:

$$d_K(N) = J^{\nu(n)\alpha(n)+\nu(n-1)\alpha(n-1)} \tag{2.39}$$

where $\alpha(i)$ represents the binary data symbols and the coefficients $\nu(i) \in \{\pm 1, 0\}$ are taken from a ternary alphabet. This gives 3^2 possible data-symbol combinations (as opposed to

the number of different values the pseudo-symbols can assume which is much smaller). If an example were completed for $L = 3$, similar to the example just worked, the pseudo-symbols would end up being

$$d_K(N) = J^{\nu(n)\alpha(n)+\nu(n-1)\alpha(n-1)+\nu(n-2)\alpha(n-2)} \tag{2.40}$$

yielding 3^3 possible pseudo-symbols. For general L, each of the pseudo-symbols are of the general form

$$d_K(N) = \prod_{i=0}^{L-1} J^{\nu(N-i)\alpha(N-i)}. \tag{2.41}$$

It can thus be seen that there are 3^L possible pseudo-symbols since there are L different binary data symbols in the product in (2.41) and since $\nu(i)$ are taken from a ternary alphabet. Therefore, weak CPM requires no more than 3^L *PAM pulses* for an exact PAM representation.

2.2.3 PAM Representation of a Special Important Case

The foregoing development uses a generic weak frequency pulse. Greater reduction in the number of pulses arises when the weak frequency pulse for an important case is used.

Pulses That are Zero

Many of the PAM pulses become zero if the frequency pulse, $f(t)$, is defined in a way that represents an important case of weak CPM. In the following derivation, only the intervals to which each pulse is time-limited will be considered as opposed to the actual behavior of the pulse during that interval.

Consider a definition of a frequency pulse, $f(t)$, of length LT, that integrates to zero:

$$\begin{aligned} f(t) &> 0 \quad 0 < t < \kappa LT \\ f(t) &< 0 \quad \kappa LT < t < LT, \end{aligned} \tag{2.42}$$

where $0 < \kappa < 1$. Referring to (2.14) it is seen that $f^+(t)$, which integrates to $1/2$, is zero for $\kappa LT < t < LT$, and $f^-(t)$, which integrates to -$1/2$, is zero for $0 < t < \kappa LT$. $g^+(t)$

and $g^-(t)$ thus become:

$$g^+(t) = \begin{cases} 0 & t < 0 \\ \frac{1}{2} & t > \kappa LT \end{cases}$$
$$g^-(t) = \begin{cases} 0 & t < \kappa LT \\ -\frac{1}{2} & t > LT \end{cases}. \tag{2.43}$$

With $g^+(t)$ and $g^-(t)$ in hand, $\Psi^+(t)$ and $\Psi^-(t)$ can both be determined which in turn determines $u^+(t)$ and $u^-(t)$.

$$\begin{aligned} u^+(t) &\neq 0 \quad 0 < t < (\kappa L + L)T \\ u^-(t) &\neq 0 \quad \kappa LT < t < 2LT. \end{aligned} \tag{2.44}$$

The latter equation will ultimately show that some PAM pulses are zero.

PAM pulse lengths Using (2.44) and (2.5) (the latter repeated in (2.45) for convenience), the length of each $C_K(t)$ and $D_K(t)$ can be calculated.

$$C_K(t) = \prod_{i=0}^{L-1} u^+(t + [i + \beta_K(i)L]T) \tag{2.45}$$
$$D_K(t) = \prod_{i=0}^{L-1} u^-(t + [i + \beta_K(i)L]T) \tag{2.46}$$
$$K = \sum_{i=1}^{L-1} 2^{i-1} \cdot \beta_K(i) \quad 0 \leq K \leq 2^{L-1} - 1 \tag{2.47}$$

For general L, consider the intervals to which $C_K(t)$ and $D_K(t)$ are time-limited:

$$C_0 \neq 0 \qquad 0 < t < (\kappa L + 1)T \tag{2.48}$$
$$D_0 \neq 0 \qquad \kappa LT < t < (L + 1)T \tag{2.49}$$
$$C_1 \neq 0 \qquad 0 < t < (\kappa L - 1)T \tag{2.50}$$
$$D_1 \neq 0 \qquad \kappa LT < t < (L - 1)T \tag{2.51}$$
$$C_2, C_3 \neq 0 \qquad 0 < t < (\kappa L - 2)T \tag{2.52}$$
$$D_2, D_3 \neq 0 \qquad \kappa LT < t < (L - 2)T \tag{2.53}$$
$$C_4, C_5, C_6, C_7 \neq 0 \qquad 0 < t < (\kappa L - 3)T \tag{2.54}$$

$$D_4, D_5, D_6, D_7 \neq 0 \qquad \kappa LT < t < (L-3)T \tag{2.55}$$

$$\vdots \tag{2.56}$$

$$C_{2^{L-1}/2}, \ldots, C_{2^{L-1}-1} \neq 0 \qquad 0 < t < (\kappa L - (L-1))T \tag{2.57}$$

$$D_{2^{L-1}/2}, \ldots, D_{2^{L-1}-1} \neq 0 \qquad \kappa LT < t < (L-(L-1))T. \tag{2.58}$$

Example for $L = 2$ Part 4

Consider once again the example for $L = 2$ by recalling (2.36):

$$\begin{aligned} s(t) =& [C_0(t)D_0(t) + C_1(t)D_1(t)] \\ &+ J^{\alpha(-1)}C_0(t)D_1(t) \\ &+ J^{\alpha(0)}[C_0(t)D_0(t+T) + C_1(t)D_0(t+2T)] \\ &+ J^{\alpha(0)+\alpha(-1)}C_0(t)D_0(t+2T) \\ &+ J^{-\alpha(-1)}C_1(t)D_0(t) \\ &+ J^{\alpha(0)-\alpha(-1)}C_1(t)D_0(t+T) \\ &+ J^{-\alpha(0)}[C_0(t+T)D_0(t) + C_0(t+T)D_1(t)] \\ &+ J^{-\alpha(0)+\alpha(-1)}C_0(t+T)D_1(t) \\ &+ J^{-\alpha(0)-\alpha(-1)}C_0(t+2T)D_0(t). \end{aligned} \tag{2.59}$$

At this point (2.48) is used to find PAM pulses that are zero. Defining the weak phase pulse as found in (2.43), it can be shown that

$$\begin{aligned} C_0 &\neq 0 \qquad 0 < t < (2\kappa+1)T \\ D_0 &\neq 0 \qquad 2\kappa T < t < 3T \end{aligned} \tag{2.60}$$

$$\begin{aligned} C_1 &\neq 0 \qquad 0 < t < (2\kappa-1)T \\ D_1 &\neq 0 \qquad 2\kappa < t < T. \end{aligned} \tag{2.61}$$

The results in (2.60) and (2.61) cause many of the pulses in (2.59) go to zero thus reducing the number of pulses in (2.36) to 4:

$$\begin{aligned} C_0(t)D_0(t+T) + C_1(t)D_0(t+2T) \neq 0 \qquad & \max[0,(2\kappa-1)T] < t < \min[(2\kappa+1)T, 2T \\ C_0(t)D_0(t+2T) \neq 0 \qquad & 0 < t < T \\ C_0(t)D_0(t) + C_1(t)D_1(t) \neq 0 \qquad & 2\kappa T < t < (2\kappa+1)T \\ C_0(t)D_1(t) \neq 0 \qquad & 2\kappa T < t < T. \end{aligned} \tag{2.62}$$

Thus the final PAM pulses for this special case of weak CPM are as follows:

$$\begin{aligned} q_0(t) &= C_0(t)D_0(t+T) + C_1(t)D_0(t+2T) \\ q_1(t) &= C_0(t)D_0(t+2T) \\ q_2(t) &= C_0(t)D_1(t) \\ q_3(t) &= C_0(t)D_0(t) + C_1(t)D_1(t). \end{aligned} \tag{2.63}$$

It can be seen from (2.36) that the pseudo-symbols corresponding to these PAM pulses in (A.73) are

$$\begin{aligned} a_0(n) &= J^{\alpha(n)} \\ a_1(n) &= J^{\alpha(n)+\alpha(n-1)} \\ a_2(n) &= J^{\alpha(n-1)} \\ a_3(n) &= J^0 = 1. \end{aligned} \tag{2.64}$$

A similar process can be applied when L is larger which will yield a similarly extensive reduction in the number of pulses. It turns out that for this special case, the number of pulses reduces to $2L$ if $\kappa = \frac{1}{L}$ (a common occurrence), which is comparable to the number of PAM pulses in the PAM decomposition of binary CPM which is equal to 2^{L-1}. Thus the number of PAM pulses increases linearly with L for weak CPM but increases exponentially with L for CPM. Indeed, $2L = 2^{L-1}$ for $L = 4$ but $2L < 2^{L-1}$ for $L > 4$!

2.2.4 Method for Forming a PAM Representation of Weak CPM

Considerable ground has been covered in order to arrive at a PAM representation for weak CPM. The final results are summarized in this section. The general PAM representation is virtually identical to Laurent's orginal PAM expression:

$$s(t) = \sum_{N=-\infty}^{\infty} \sum_{K=0}^{P-1} d_K(N) g_K(t - NT). \tag{2.65}$$

A substantial amount of work has been put into finding a closed form for the pseudo-symbols, $d_K(N)$, and the PAM pulses, $g_K(t)$. For example, Mengali presented an extensive algorithm used to calculate the pseudo-symbols and PAM pulses. In the case of weak CPM this algorithm, which was used to derive the PAM representation, leaves open the question of the length of each pulse and of the form of the pseudo-symbols. This extra level of complexity beyond that required to form Laurent's PAM decomposition, is no greater than the complexity required to calculate the pulses by hand. An approach to computing the PAM pulses and pseudo-symbols of a complexity comparable to Mengali's algorithm is therefore a brute-force approach. Once the pulses are calculated, simplification of the exact representation can then be completed.

As discussed in the process of the derviation, at most, there will be 3^L PAM pulses for a given representation. A further reduction in the number of pulses comes when weak CPM uses an important common form of weak frequency pulses, as discussed in Section 2.2.3. Indeed, all indications suggest that the number of PAM pulses for weak CPM can be reduced to as few as $2L$, which is comparable to (and less than for larger values of L) the number of pulses in Laurent's PAM representations of CPM.

The algorithm chosen is as follows. First, calculate the PAM pulses $C_K(t)$ (based on $g^+(t)$) and $D_K(t)$ (based on $-g^-(t)$). This requires that $g^+(t)$ and $g^-(t)$ be calculated first,

and therefore also requires formation of $f^+(t)$ and $f^-(t)$, using the following equations:

$$f^+(t) = \begin{cases} f(t) & f(t) > 0 \\ 0 & \text{otherwise} \end{cases}$$
$$f^-(t) = \begin{cases} f(t) & f(t) < 0 \\ 0 & \text{otherwise} \end{cases} \tag{2.66}$$

$$g^{\pm}(t) = \int_{-\infty}^{t} f^{\pm}(\tau)\, d\tau. \tag{2.67}$$

This allows the calculation of $\Psi^+(t)$ and $\Psi^-(t)$ and subsequently $u^+(t)$ and $u^-(t)$, the latter two functions being the basis of the PAM representation:

$$\Psi^+(t) = \begin{cases} g^+(t) & 0 < t < LT \\ 2\pi h - \pi h g^+(t) & LT < t < 2LT \end{cases} \tag{2.68}$$

and

$$\Psi^-(t) = \begin{cases} -g^-(t) & 0 < t < LT \\ 2\pi h + \pi h g^-(t) & LT < t < 2LT \end{cases} \tag{2.69}$$

$$u^+(t) = \frac{\sin[\Psi^+(t)]}{\sin(\pi h)} \tag{2.70}$$

$$u^-(t) = \frac{\sin[\Psi^-(t)]}{\sin(\pi h)}. \tag{2.71}$$

Finally, the PAM pulses based on $u^+(t)$ and $u^-(t)$ can be formed:

$$C_K(t) = \prod_{i=0}^{L-1} u^+(t + [i + \beta_K(i)L]T) \tag{2.72}$$

$$D_K(t) = \prod_{i=0}^{L-1} u^-(t + [i + \beta_K(i)L]T). \tag{2.73}$$

$\beta_K(i)$ is the i-th coefficient for the radix-2 decomposition of an integer K, as seen in the following:

$$K = \sum_{i=1}^{L-1} 2^{i-1} \cdot \beta_K(i) \qquad 0 \le K \le 2^{L-1}. \tag{2.74}$$

Next, the product of the PAM representations of two CPM signals is formed and expanded:

$$s(t) = \sum_{N=-\infty}^{\infty} \sum_{K=0}^{2^{L-1}-1} a_K(N) C_K(t - NT) \cdot \sum_{N'=-\infty}^{\infty} \sum_{K'=0}^{2^{L-1}-1} a^*_{K'}(N') D_{K'}(t - N'T). \quad (2.75)$$

New pulses are thus formed as products of $C_K(t+NT)$ and $D_{K'}(t+N'T)$ for all possible permutations of K, K', N, and N', as demonstrated in (2.19). A particular bit time is chosen and any pulses whose region of support began in previous bit times will be discarded, as explained in Section 2.2.1 in conjuction with (2.19). Pulses with identical pseudo-symbol coefficients are grouped to effect simplifications possible regardless of the frequency pulse used in defining the weak CPM signal. At this point, there will be no more than 3^L unique PAM pulses.

If $f(t)$ is as defined in (2.42), further simplification is possible. The time-limited nature of $C_K(t)$ and $D_K(t)$, as shown in (2.48), can be examined along with (2.42) to discover and eliminate pulses that are zero; these two equations are repeated here for convenience:

$$\begin{aligned}
C_0 &\neq 0 \qquad 0 < t < (\kappa L + 1)T \\
D_0 &\neq 0 \qquad \kappa LT < t < (L+1)T \\
C_1 &\neq 0 \qquad 0 < t < (\kappa L - 1)T \\
D_1 &\neq 0 \qquad \kappa LT < t < (L-1)T \\
C_2, C_3 &\neq 0 \qquad 0 < t < (\kappa L - 2)T \\
D_2, D_3 &\neq 0 \qquad \kappa LT < t < (L-2)T \\
C_4, C_5, C_6, C_7 &\neq 0 \qquad 0 < t < (\kappa L - 3)T \\
D_4, D_5, D_6, D_7 &\neq 0 \qquad \kappa LT < t < (L-3)T \\
&\vdots \\
C_{2^{L-1}/2}, \ldots, C_{2^{L-1}-1} &\neq 0 \qquad 0 < t < (\kappa L - (L-1))T \\
D_{2^{L-1}/2}, \ldots, D_{2^{L-1}-1} &\neq 0 \qquad \kappa LT < t < (L - (L-1))T
\end{aligned} \quad (2.76)$$

$$\begin{aligned}
f(t) &> 0 \quad 0 < t < \kappa LT \\
f(t) &< 0 \quad \kappa LT < t < LT.
\end{aligned} \quad (2.77)$$

This elimination results in limiting the number of PAM pulses to as few as $2L$ where $2L$ is reached when $\kappa = 1/L$.

2.3 Application to EFTS

The EFTS signal has the following design requirements. The peak frequency deviation, f_d, is 60 kHz. The bit rate, R_b, is 7200 bits per second (bps). The modulation type is continuous-phase modulation, using a Manchester frequency pulse. Before the frequency pulse train is input into an FM modulator to create the CPM signal, EFTS dictates the frequency-pulse train is to be filtered by a 4-pole low-pass Bessel filter with cut-off frequency $F_c = 15$ kHz.

These parameters need to be converted into the model used for simulating the CPM modulator modeled in Chapter 1. The model requires the modulation index, h, defined in [23, section 4.3.3] as

$$h = 2f_dT \tag{2.78}$$

where T is the symbol time, which for a binary modulation is equal to the bit time, T_b. The bit time can be calculated as

$$T_b = \frac{1\frac{\text{bit}}{\text{symbol}}}{R_b\left(\frac{\text{bits}}{\text{second}}\right)} = \frac{1}{R_b}; \tag{2.79}$$

$$\text{therefore, } h = 16.66\bar{6}. \tag{2.80}$$

The model chosen to represent the low-pass Bessel filter was a Gaussian low-pass filter with $F_c = 15$ kHz. This choice was made for two reasons. First, the Gaussian low-pass filter is used as the pre-modulation filter for GMSK [25] where GMSK is CPM based on an NRZ frequency pulse, filtered by a low-pass Gaussian filter with a time-bandwidth BT, and with $h = \frac{1}{2}$. This is interesting because GMSK provides approximately the same spectral shaping as the recommended EFTS pre-modulation filter. Second, the Gaussian low-pass filter produces a somewhat more tractable mathematical expression for the frequency, and phase pulses, compared to when using a Bessel filter.

The frequency and phase pulses may be expressed as

$$f(t) = \chi\sqrt{2\pi}\sigma h \left[2Q\left(\frac{t - LT/2}{\sigma}\right) - Q\left(\frac{t-(L-1)T/2}{\sigma}\right) - Q\left(\frac{t-(L+1)T/2}{\sigma}\right)\right] \quad (2.81)$$

$$\begin{aligned} g(t) = \chi\pi h \Bigg[& \sigma\left(e^{-\frac{1}{2}\left(\frac{t-(L+1)T/2}{\sigma}\right)^2} - e^{-\left(\frac{(L+1)T)}{2\sigma}\right)^2}\right) \\ & + \sqrt{2\pi}\left(t - \frac{(L+1)T}{2\sigma}\right) Q\left(\frac{t-(L+1)T/2}{\sigma^2}\right) \\ & + \sqrt{2\pi}\frac{(L+1)T}{2} Q\left(-\frac{(L+1)T}{2\sigma}\right) \\ & + \sigma\left(e^{-\frac{1}{2}\left(\frac{t-(L-1)T/2}{\sigma}\right)^2} - e^{-\left(\frac{(L-1)T)}{2\sigma}\right)^2}\right) \\ & + \sqrt{2\pi}\left(t - \frac{(L-1)T}{2\sigma}\right) Q\left(\frac{t-(L-1)T/2}{\sigma^2}\right) \\ & + \sqrt{2\pi}\frac{(L-1)T}{2} Q\left(-\frac{(L-1)T}{2\sigma}\right) \\ & - 2\sigma\left(e^{-\frac{1}{2}\left(\frac{t-LT/2}{\sigma}\right)^2} - e^{-\left(\frac{LT}{2\sigma}\right)^2}\right) \\ & - 2\sqrt{2\pi}\left(t - \frac{LT}{2\sigma}\right) Q\left(\frac{t-LT/2}{\sigma^2}\right) - 2\sqrt{2\pi}\frac{LT}{2} Q\left(-\frac{LT}{2\sigma}\right)\Bigg] \end{aligned} \quad (2.82)$$

where

$$Q(x) = \frac{1}{\sqrt{2\pi}}\int_x^\infty e^{-u^2/2}du, \quad (2.83)$$

$$\sigma = \frac{\sqrt{\ln 2}}{2\pi B}, \quad (2.84)$$

and χ is a constant required to produce the desired frequency deviation.

As stated, the modulation for this model is similar to Gaussian minimum-shift keying (GMSK). Recall that L is the number of symbol periods spanned by the frequency pulse. Tsai and Lui [26] give the following approximation for L in GMSK as a function of BT:

$$L \approx \left\lceil \frac{1}{BT} \right\rceil \quad (2.85)$$

where $\lceil \cdot \rceil$ denotes the integer closest to and larger than $(\cdot)$. For the model used by EFTS,

$$\begin{aligned} BT &= B \cdot T_b \\ &= \frac{15\,\text{kHz}}{R_b} \\ &= \frac{15\,\text{kHz}}{7.2\,\text{kBps}} = 2.08\bar{3}. \end{aligned} \tag{2.86}$$

It turns out that a slightly different approximation should be used for EFTS, as can be seen in Figure 1.1, which is a Manchester frequency pulse filtered by a Gaussian low-pass filter with $BT = 2.08\bar{3}$. This figure shows that the pulse spans somewhere between one and two symbol times. Thus for this case, L can be calculated as,

$$L \approx 2 \left\lceil \frac{1}{BT} \right\rceil = 2. \tag{2.87}$$

Since $L = 2$ and $\kappa = \frac{1}{2}$ (as used in (2.77)), (2.62) shows that

$$\begin{aligned} q_0(t + nT) &= C_0(t + nT)D_0(t + (n+1)T) \neq 0 \qquad 0 < t < 2T, \\ q_1(t + nT) &= C_0(t + nT)D_0(t + (n+2)T) \neq 0 \qquad 0 < t < T, \\ \text{and } q_2(t + nT) &= C_0(t + nT)D_0(t + nT) \neq 0 \qquad T < t < 2T \end{aligned} \tag{2.88}$$

are the appropriate PAM pulses for an exact representation of EFTS-based CPM, shown in Figure 2.1 with their spectra shown in Figure 2.2. It can be seen from (2.64) that the respective pseudo-symbols for these PAM pulses are

$$\begin{aligned} a_0(n) &= J^{\alpha(n)} \\ a_1(n) &= J^{\alpha(n)+\alpha(n-1)} \\ a_2(n) &= J^0 = 1. \end{aligned} \tag{2.89}$$

Thus, the PAM representation of EFTS PAM is

$$s(t) = \sum_{N=-\infty}^{\infty} (e^{j\pi h\alpha(n)} q_0(t - NT) + e^{j\pi h[\alpha(n)+\alpha(n-1)]} q_1(t - NT) + q_2(t - NT). \tag{2.90}$$

2.4 Power Spectrum of Weak CPM Using the PAM Representation

The PAM representation of weak CPM aids in understanding the undesirable frequency spectrum characteristics in weak CPM. Anderson, Aulin and Sundberg state that

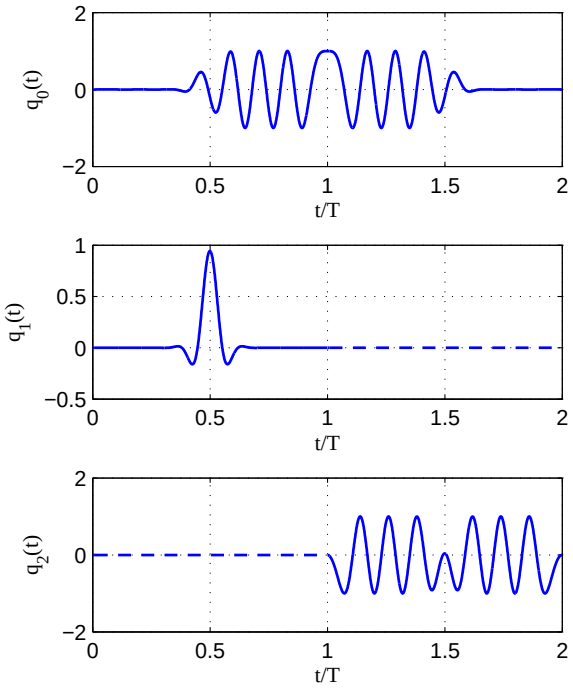

Figure 2.1: The three PAM pulses $q_0(t)$, $q_1(t)$, and $q_2(t)$ in the PAM representation of the EFTS waveform.

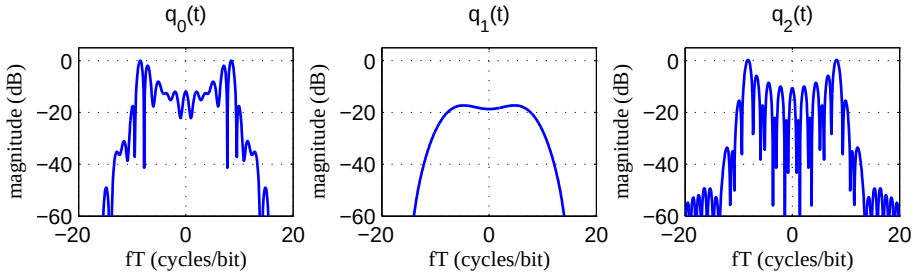

Figure 2.2: The spectra of the three PAM pulses $q_0(t)$, $q_1(t)$, and $q_2(t)$ in the PAM representation of the EFTS waveform.

weak CPM has discrete lines in its power spectral density (PSD). They further state that these lines are undesirable, because they represent wasted transmit power since they contain no information [9, page 154].

A periodic function has discrete lines, or impulses, in its Fourier Transform; the magnitude of each of these impulses is proportional to the Fourier-series coefficients of the periodic function [27, Section 4.2]. Thus, if an autocorrelation function has a periodic component, the PSD, which is the Fourier transform of the autocorrelation function, will have discrete lines.

This understanding combined with the PAM representation provides a way to discover the presence of discrete lines in weak CPM, different from that found in [9]. As seen in (2.36), when $L = 2$ one of the PAM components is symbol-independent, which is deterministic; such a pulse surfaces in the PAM representation of weak CPM regardless of the value of L. A function made up of such a deterministic pulse repeated at regular intervals is periodic. Since one of the PAM pulses of weak CPM is always symbol-independent, (2.65) shows that there is a time-shifted version of this symbol-independent pulse in every symbol interval, thus giving $s(t)$ a periodic component. The presence of this periodic component also implies the presence of a periodic component in the autocorrelation function, ultimately resulting in discrete lines in the PSD.

Example for $L = 2$ Part 5

Consider the symbol-independent pulse associated with the $L = 2$ example:

$$q_i(t) = C_0(t)D_0(t) + C_1(t)D_1(t) \tag{2.91}$$

where i will be chosen based on the number of pulses that are present in the PAM representation. In forming the autocorrelation of the CPM signal,

$$\phi_{ss}(t, t+\theta) = \mathrm{E}\left\{s(t)s^*(t+\theta)\right\}, \tag{2.92}$$

$q_i(t)$ will remain symbol-independent only when placed in a product with shifted versions of itself.

Assuming the frequency pulse is defined as

$$\begin{aligned} f(t) > 0 \quad 0 < t < \frac{LT}{2} \\ f(t) < 0 \quad \frac{LT}{2} < t < LT \end{aligned} \tag{2.93}$$

which is of the form of (2.42), $q_i(t)$ is time-limited to $T < t < 2T$. The periodic pulse present in the autocorrelation in this special case of $L = 2$ is therefore

$$\phi_{\text{ss,periodic}}(t, t+\theta) = \sum_N q_i(t+NT)\{q_i(t+\theta+NT) + q_i(t+\theta+[N+1]T)\} \tag{2.94}$$

where $0 \leq \theta < T$. The region of support of this periodic pulse is

$$NT < t < (N+1)T, \tag{2.95}$$

and so has a period of T. The autocorrelation function, $\phi_{\text{ss}}(t, t+\theta)$, represents the periodic part of a cyclo-stationary random process, and thus $\phi_{\text{ss,periodic}}(t, t+\theta)$ makes up a part of a cyclo-stationary random process. In order to calculate the PSD by taking the Fourier transform of the autocorrelation function, the autocorrelation function must represent a stationary random process (i.e. it must be a function of only one variable). The common practice used to convert the autocorrelation function of a cyclo-stationary random process into the autocorrelation function of a stationary random process is to average over one period of the autocorrelation function [23]. Thus

$$\phi_{\text{ss,periodic}}(\theta) = \frac{1}{T}\int_{NT}^{(N+1)T} \phi_{\text{ss,periodic}}(t, t+\theta)\, dt \tag{2.96}$$

represents a stationary random process. The discrete lines due to (2.94) can thus be calculated using the following equation [27],

$$\begin{aligned} X(f) &= \sum_{k=-\infty}^{\infty} b_k \delta(f - 1/T) \\ \text{where } b_k &= \frac{1}{T}\int_T \phi_{\text{ss,periodic}}(\theta) e^{-j\frac{k}{T}\theta}\, d\theta. \end{aligned} \tag{2.97}$$

The latter part of (2.97) represents the Fourier series coefficients of $\phi_{\text{ss,periodic}}(\theta)$.

A PAM representation for weak CPM has now been developed; the next step is to see how this PAM representation can be used to build a PAM-based receiver and how to predict the performance of such a receiver, and finally, predict and simulate the receiver's performance.

Chapter 3

Weak CPM Receivers

The main interest in a PAM representation of CPM arises in the design of the receiver, which seeks to detect the transmitted data sequence from the received signal $r(t)$:

$$r(t) = s(t) + w(t). \tag{3.1}$$

This received signal consists of the transmitted signal, $s(t)$, plus noise $w(t)$, modeled as additive white Gaussian noise (AWGN). An optimal way, in terms of bit-error rate (BER), to effect this detection is through the use of a maximum likelihood sequence detector (MLSD), which is a detector that performs maximum likelihood sequence estimation (MLSE). This detector requires a sometimes prohibitively high complexity; it is therefore desirable to use a sub-optimum detector which requires a lower level of complexity. The use of a PAM-based representation of CPM is one method that allows reduction in the complexity of the receiver. (For other methods, see [9, chapter 8].) The act of reformulating weak CPM as a PAM signal does not alone provide for a reduced complexity receiver. Indeed, a receiver built using all of the PAM pulses to detect the signal is just another formulation of MLSE [24], which is of roughly the same complexity as the MLSE detector for CPM described in [9, page 249]. On the other hand, using fewer PAM pulses than the number required for an exact representation (i.e. using an approximate representation) does decrease complexity without a significant drop in BER; even a receiver using only the most energetic PAM pulse greatly outperforms an FM limiter-discriminator detector.

Section 3.1 reviews maximum-likelihood (ML) detectors and Section 3.2 outlines the design of sub-optimum detectors. Section 3.3 applies the results of the first two sections

to the EFTS waveform. Finally, Section 3.4 presents simulation results and complexity comparisons of the various EFTS detectors.

3.1 Maximum Likelihood Detection

In order to understand how a MLSD works, it will be helpful to describe CPM using a phase-state trellis, which is defined based on the phase states, correlative states, and state transition of CPM.

States In weak CPM, the trellis arises when the frequency pulse spans more than one symbol time. Within the trellis structure, there are *phase states*, which represent accumulated phase due to previous data symbols which are no longer transitioning; in weak CPM, there is only one phase state, since the accumulated phase is zero. There are also *correlative states* based on previous symbols that are still transitioning; there are thus 2^{L-1} (M^{L-1} for M-ary CPM) possible correlative states. The correlative states and the phase states are combined into a *state vector*; each trellis state is described by a unique state vector. There are two paths leaving each state (M paths for M-ary CPM). The *state transition*, which is based on the current symbol, describes these paths; the current data symbol determines to which of the two possible states these paths lead. Using the state vector and the state transition, a trellis can be constructed to show all possible states and state transitions. This will be done for EFTS later on in this chapter.

3.1.1 ML Detection Using the Complex Exponential Representation

A MLSD searches for the path through the phase state trellis which most closely represents the path taken by the transmitted signal. "Most closely resembles" in this case (signal + AWGN) means that the signal representing the path chosen as the most likely path is less different to the received signal in terms of squared Euclidean distance than a signal representing any other path through the trellis. A metric that performs this search is

$$\arg\max_{\tilde{\boldsymbol{\alpha}}} \left\{ \ln \left[p_{r(t)|\tilde{\boldsymbol{\alpha}}}(r(t)|\tilde{\boldsymbol{\alpha}}) \right] \right\} = \arg\min_{\tilde{\boldsymbol{\alpha}}} \left\{ \int_{-\infty}^{\infty} |r(t) - s(t, \tilde{\boldsymbol{\alpha}})|^2 \, dt \right\} \tag{3.2}$$

where $\tilde{\boldsymbol{\alpha}}$ represents a possible transmitted sequence. (Equation 3.2 is simply the log-likelihood function for some signal in the AWGN channel.) The squared term in (3.2)

is expanded and only the pieces that vary with $\tilde{\boldsymbol{\alpha}}$ are considered. This yields an equation equivalent to (3.2):

$$\arg\max_{\tilde{\boldsymbol{\alpha}}} \Lambda(\tilde{\boldsymbol{\alpha}}) = \arg\max_{\tilde{\boldsymbol{\alpha}}} \mathrm{Re}\left\{ \int_{-\infty}^{\infty} r(t) s^*(t, \tilde{\boldsymbol{\alpha}})\, dt \right\}. \tag{3.3}$$

This metric assumes the whole received signal is in hand before a decision is made. The Viterbi Algorithm, on the other hand, calculates this metric piece-meal so as to enable the making of decisions as the signal arrives.

The Viterbi Algorithm

The Viterbi Algorithm splits up the decision by incorporating newly received information one symbol time at a time as follows:

$$\arg\max_{\tilde{\boldsymbol{\alpha}}} \mathrm{Re}\{\Lambda_j(n; \tilde{\boldsymbol{\alpha}})\} = \arg\max_{\tilde{\boldsymbol{\alpha}}} \left\{ \Lambda_i(n-1; \tilde{\boldsymbol{\alpha}}) + \mathrm{Re}[\lambda_{m,i}(n; \tilde{\boldsymbol{\alpha}}_n)] \right\} \tag{3.4}$$

$$\lambda_{m,i}(n; \tilde{\boldsymbol{\alpha}}_n) = \int_{nT}^{(n+1)T} r(t) s_m^*(t, \tilde{\boldsymbol{\alpha}}_n)\, dt \tag{3.5}$$

where $\tilde{\boldsymbol{\alpha}}_n = \{\alpha(n), \alpha(n-1), \ldots, \alpha(n-[L-1])\}$ is a possible data sequence based on the symbols from time $n-(L-1)$ up to and including time n.

Two comments about (3.4) will be instructive. First, the integral in (3.4) simply represents a matched filtering of $r(t)$ by filters matched to the possible CPM waveforms in the interval $nT < t < (n+1)T$. The second comment regards the metrics uses in (3.4). $\lambda_{m,i}$ is the recursive metric and Λ is the cumulative metric [9, page 249]. Λ represents the metric for a given state, and since there are 2^{L-1} trellis states, there are 2^{L-1} different Λ metrics, thus i and j in the subscripts of (3.4) each take on a different value in the range $0 \le i, j \le 2^{L-1}-1$. Also, $\lambda_{m,i}$ represents the metrics for each of the two paths leaving each of the states. Equation (3.4) shows that $\lambda_{m,i}$ is a function of the previous $L-1$ symbols and the current symbol, so there are 2^L different recursive metrics to be calculated each symbol time. In order to allow for 2^L combinations, m ranges as $0 \le m \le 1$, since i is in the range $0 \le i \le 2^{L-1}-1$; i.e., since there are 2^{L-1} trellis states and there are 2 paths leaving each state, there must be 2^L different paths and so there must be an equal number of metrics to describe these paths.

Incorporating new information one symbol time at a time is only half of the story. At this point, the number of paths still grows exponentially with each additional symbol time. The Viterbi Algorithm uses the following scoring method to eliminate unnecessary paths, reducing to a great degree the complexity required to determine the most likely data sequence. It will be seen that the Viterbi Algorithm fixes the path length and the number of maintained paths. (MLSE detection in the form shown in (3.3) requires a number of paths that grows exponentially with the length of the transmitted sequence).

The cumulative metric, Λ_i, represents the information contained in the i-th state vector and recursive metric, $\lambda_{m,i}$, represents the information relative to the two phase transitions leaving the i-th state. That is, Λ_i gives a "score" to each of the possible state vectors. Then each of the possible paths leaving each of the states is assigned a score equal to $\lambda_{m,i}$. The total score for a path leaving the state is equal to $\lambda_{m,i} + \Lambda_i$.

Each path transitions to some state where it will merge with a path that left from a different state. The scores of these two paths are compared and the path with the larger score is declared the survivor; the other path is discarded. The destination state is assigned a new score, equal to the sum of metrics corresponding to the surviving path:

$$\Lambda_j(n; \tilde{\boldsymbol{\alpha}}) = \lambda_{m,i}(n; \tilde{\boldsymbol{\alpha}}_{L-1}) + \Lambda_i(n-1; \tilde{\boldsymbol{\alpha}}). \tag{3.6}$$

The discarded path no longer holds any useful information since any path leaving the j-th state will increase its score the same amount, regardless of the value of the Λ_i and $\lambda_{i,m}$ of the surviving path. Therefore, the discarded path will always have a smaller cumulative score than the survivor.

In fine, the Viterbi Algorithm operates along the following four steps to keep the computational complexity manageable. First, the recursive metrics in (3.5) is calculated in order to incorporate the new information that just arrived at the receiver, second, these metrics are added to their associated cumulative metrics, third, metrics of merging paths are compared, and fourth, a soft decision is made by declaring the larger of the two metrics as the survivor and the path with the smaller metric is discarded. The number of possible paths is thus maintained at 2^L different paths and the computational load is spread out over the length of the transmitted sequence. Up to this point, the trellis paths have been followed

and the most likely paths, up to the current time, $(n+1)T$, (or n-th symbol time) have been isolated.

When the received signal has been observed over a sufficiently long[1] interval of time and the recorded paths contain information about the first n symbol times, a hard decision about the first bit is made. The first symbol interval in the path, which corresponds to this hard decision, can then be removed and disregarded. The recorded paths will then cover $n-1$ symbol periods. From this point on, the algorithm produces one bit every symbol time by sliding the observation window.

The sliding operation happens in the following four recursive steps. 1) The first hard decision is made. 2) After the first decision is made, the part of the path regarding the decision is removed leaving path information about the 2^{nd} symbol interval up to the n-th symbol interval. 3) Following this removal, an additional time interval is added to the mix by calculating the next metric using (3.5), adding the $(n+1)$-th interval to the path information. 4) The Viterbi Algorithm then makes soft decisions (using the four steps described in the preceding paragraph), eliminating half of the paths opening the way for another hard decision to be made and so the process repeats. Thus, the complexity is greatly reduced, and the path length is set at a length of n. Furthermore, the Viterbi Algorithm only needs to keep track of 2^L paths of this length, instead of a number of paths which grows exponentially with the number of symbol times observed.

An example of receivers using the Viterbi Algorirhtm and the other following receivers will be given later in this chapter.

Analysis: Minimum Euclidean Distance and Naming Weak CPM

In discussing receivers, interest lies most heavily in performance; a method for predicting receiver performance will now be presented.

[1]"Sufficiently long" refers to the fact that after several cycles, the first bit of all paths will be the same with an asymptotic probability of 1. To find the number of these cycles that quanlifies as sufficiently long, the detector can be designed and tested with increasingly long observation intervals. (The observation interval refers to the number, n, of symbol times the receiver is allowed to observe, while making soft decisions, before a hard decision is made.) When increasing the length of the observation interval no longer reduces the BER, the observation interval is "sufficiently long."

The first step in the presentation is to discuss the notion of a union bound. The union bound of probability says that the probability of the union of events occurring is less than or equal to the sum of the individual probability of each of those events. Using the union bound on pair-wise error probabilities yields the following inequality for the probability of error for CPM in the AWGN channel:

$$P_b \leq \sum_i \sum_{j \neq i} Q\left(\sqrt{d_{ij}^2 \frac{E_b}{N_0}}\right) \tag{3.7}$$

where $Q\left(\sqrt{d_{ij}^2 \frac{E_b}{N_0}}\right)$ is the probability that the sequence estimate is $\boldsymbol{\alpha}_j$ when $\boldsymbol{\alpha}_i$ was transmitted and d_{ij}^2 is the Euclidean distance between $\boldsymbol{\alpha}_j$ when $\boldsymbol{\alpha}_i$ given by

$$d_{ij}^2 = \frac{1}{2E_b} \int |s(t, \boldsymbol{\alpha}_i) - s(t, \boldsymbol{\alpha}_j)|^2 \, dt. \tag{3.8}$$

If the double sum in (3.7) is reordered so as to combine terms that have equal Euclidean distances, the result is

$$P_b \leq \sum_i \sum_{j \neq i} Q\left(\sqrt{d_{ij}^2 \frac{E_b}{N_0}}\right) = \sum_k W_k Q\left(\sqrt{d_k^2 \frac{E_b}{N_0}}\right) \tag{3.9}$$

where d_k is some Euclidean distance between two sequences and W_k is a function of the number of sequence pairs that have a Euclidean distance of d_k. P_b as defined in (3.9) is dominated by the term corresponding to the smallest distance:

$$d_{\min}^2 = \min_k \left\{ d_k^2 \right\}. \tag{3.10}$$

At high SNR, (3.9) can be approximated as

$$P_b \approx W_{\min} Q\left(\sqrt{d_{\min}^2 \frac{E_b}{N_0}}\right). \tag{3.11}$$

$W_{\min}$ becomes insignificant at high SNR [9, pages 27,28,55,59]. (Note that the accuracy of this approximation decreases as the difference between $d_{\min}^2$ and the next largest d^2 becomes relatively small.)

Consider the following example. Minimum-shift keying (MSK) is CPM with $h = \frac{1}{2}$ and a non-return to zero (NRZ) frequency pulse of length T; MSK has a $d_{\min}^2 = 2$, which translates to an expected probability of error of $P_b \approx 3.9 \times 10^{-6}$ at an $E_b/N_0 = 10$ dB. One

version of weak CPM could use the same h but replace the frequency pulse with a length-T *Manchester* frequency pulse; this modulation has a $d^2_{\text{min}} \approx 0.36$, which translates to an expected probability of error of $P_b \approx 2.9 \times 10^{-2}$ at an $E_b/N_0 = 10$ dB. This difference in Euclidean distances results in a loss of 7.47 dB at a $P_b = 10^{-6}$. *This makes clear the reasoning behind the name "weak CPM."*

Complexity

The number of real multiplies and real additions required will now be used to consider this receiver's complexity. In doing so, keep in mind that 1) the complex-envelope was used to simulate the receiver, and so complex multplies were required, that 2) a complex multiply requires four real multiplies and two real adds, and that 3) if there are X multiplies in a filtering operation, there are $X - 1$ adds.

The complex exponential-based MLSD receiver requires as many length-T matched filters as it has recursive metrics. Equation (3.4) shows that there are 2^L such metrics. Assuming N samples per bit are used for the digital realization of the system, each filter requires N complex multiplies. Each complex multiply requires four real multiplies and two real adds, but as the imaginary part is discarded, there are just two real multiplies and one real add.[2] Thus, $2^L N$ complex multiplies are required, but only $2^{L+1}N$ real multiplies and $2^L(2N-1)$ real adds ($2N-1$ real adds for each T-length filter). To summarize, this detector requires

$$2^{L+1}N \tag{3.12}$$

real multiplies and

$$2^L(2N-1) \tag{3.13}$$

real adds. The complexity required for effecting MLSE must also be accounted for, but will not be quantified here.

[2] If $x = x_r + jx_i$ and $y = y_r + jy_i$ are complex numbers then $xy = x_r y_r - x_i y_i + j(x_r y_i + x_i y_i)$. So if the imaginary part is discarded, only two real multiplies and one real add are necessary.

3.1.2 ML Detection Using the PAM Representation

An optimum receiver for a PAM-based modulation uses a matched filter [23]; for this reason, Kaleh designed a MLSD that uses matched filters based on the PAM pulses to compute the recursive metric [24].

Calculating the metrics for Kaleh's method boils down to the following process, which also uses the Viterbi Algorithm and consists of six steps. First, the received signal is fed into a bank of matched filters, which correspond to each of the PAM pulses and which are sampled at times $t = nT$. The k-th matched-filter output at time nT is

$$\eta_k(n) = \int_{-\infty}^{t} r(\tau) h_k(\tau)\, d\tau \Big|_{t=nT} \tag{3.14}$$

where $h_k(t)$ is a matched-filter based on the k-th PAM pulse. (Note that at time nT, the signal is only based on symbols up to and including the $(n-1)$-th symbol.) Second, the k-th filter output is multiplied by the k-th pseudo-symbol, the latter being based on one of the possible data sequences. Third, the real part of the sum of these products is taken yielding the recursive metric:

$$\lambda_{m,i}(n) = \text{Re}\left\{ \sum_{k=0}^{P-1} \eta_k(n) d^*_{i,k}(n) \right\}, \tag{3.15}$$

where * denotes complex conjugation, P is the total number of PAM pulses, and m represents the two possible transition paths. Fourth, these recursive metrics are summed to form the cumulative metric

$$\Lambda_j(n) = \sqrt{2E_b} \sum_{l=-\infty}^{n} \lambda_{m,i}(l) \tag{3.16}$$

which lends itself easily to the recursive formulation

$$\Lambda_j(n) = \Lambda_i(n-1) + \sqrt{2E_b}\lambda_{m,i}(n) \tag{3.17}$$

where n means the n-th symbol time is being considered (i.e., the time interval $nT < t < (n+1)T$). The variable i represents one of the 2^{L-1} possible states; that is Λ_i represents the metric for the i-th state and m represents one of two possible path transitions. Fifth, as with the complex exponential-based receiver, $\Lambda_i(n)$ must be calculated for each of the states after which it is added to each $\lambda_{m,i}(n)$ to find the metrics for each of the paths leaving each

of the states. Sixth, the metrics of merging paths are compared to find the survivors and to discard the other paths. Just as with the CPM MLSD, after a sufficiently long observation interval, hard decisions can begin to be made on the bits.

Analysis

Since this detector is simply another instance of a MLSD, the minimum distance for this receiver will be the same as it was for the exponential-based ML detector.

Complexity

Equations (3.15) and (3.17) show the metrics calculated by the PAM-based MLSD. The PAM-based MLSD receiver requires a matched filter of length $\Omega_i T$ for each PAM pulse, where Ω_i is the number of bit times spanned by the i-th PAM pulse. The PAM matched filters are real-valued filters but the received signal is complex so this receiver requires

$$\Upsilon = 2N \sum_{i=0}^{P-1} \Omega_i \tag{3.18}$$

real multiplies and no adds,[3] again assuming N samples/bit are used for the digital realization of the system. After these multiplies, the complex output of each matched filter is multiplied by the possible pseudo-symbol combinations and the imaginary part is discarded. If the i-th pseudo-symbol, which corresponds to the i-th PAM pulse, is a function of Θ_i different data symbols, then there are

$$\Phi = \sum_{i=0}^{P-1} 2^{\Theta_i} \tag{3.19}$$

real adds and 2Φ real multiplies required to calculate the metrics $\lambda_{m,i}$. Thus the ML PAM-based detector requires

$$\Upsilon + 2\Phi \tag{3.20}$$

real multiplies and Φ real adds. Just as with the ML complex exponential-based detector, the complexity required to effect MLSE must be taken into account.

[3] If $x = x_r$ is a real number and $y = y_r + jy_i$ is a complex number then $xy = x_r y_r + jx_r y_i$. So there are only two real multiplies required but no adds are required.

3.2 Sub-Optimum Detection

Two sub-optimum receivers were used in the simulations. One was a PAM-based receiver, using only the most energetic symbol-dependent pulse. The other receiver is a FM limiter-discriminator since CPM can be viewed as "digital FM" [28] and since the current EFTS uses an FM demodulator at the receiver.

3.2.1 Reduced-Complexity Detection Using the PAM Representation

Simplified PAM receivers have been studied by Kaleh [24] and Tsai and Lui [26, 29] for GMSK, by Colavolpe and Raheli [30] for M-ary CPM, and by Perrins and Rice [13] for M-ary multi-h CPM.

The cumulative metric for the ML detectors as as well as the process for calculating their metrics is the same with this detector excepting the computation of the recursive metric, which changes (3.15) to

$$\lambda_{m,i}(n) = \text{Re}\left\{\sum_{k=0}^{R-1} \eta_k(n) d_{i,k}^*(n)\right\}, \tag{3.21}$$

where R is some integer less than P, the total number of PAM pulses, and R represents the number of PAM pulses that will be kept in making the simplified receiver. Thus, the sum now only sums from 0 to $R-1$ instead of 0 to $P-1$; the variables m and i will now vary to account for all the possible combinations of data symbols that are used in the reduced set of pseudo-symbols.

This change may or may not affect the trellis. The trellis will change only if the reduction in the number of pulses and corresponding reduction in the number of pseudo-symbols results in the complete removal of one of the data symbols. For example, suppose that the exact PAM representation of some weak CPM signal depends on the current and previous two data symbols. The MLSE trellis will have four states and two transitions out of each of those states. Then, if an approximate representation is used which is dependent only on the current and previous data symbol, the trellis will have only two states and two transitions from each of these states. Finally, if an approximation depends only on the current data symbol, the trellis disappears entirely, and a symbol-by-symbol detector will

suffice. (An example of this latter case will be shown in designing the EFTS simplified receiver.)

Analysis: Mismatched Filter

If the receiver is not matched exactly to the transmitted signal, then a mismatched Euclidean distance must be used to compare receiver configurations. This situation arises when a simplified PAM receiver is used, which uses an approximate PAM signal, represented by a slightly modified version of (2.37):

$$\tilde{r}(t) = \sum_{N=-\infty}^{\infty} \sum_{K=0}^{R-1} a_{K,N} C_K(t - NT) \tag{3.22}$$

where R is some integer less than P, the total number of PAM pulses. The probability of error is well approximated by (3.11) except that $d^2_{\min}$ is replaced by a modified distance measure given by

$$\tilde{d}^2 = \frac{1}{\sqrt{2E_b}} \frac{\left(\int |\tilde{s}(t;\boldsymbol{\alpha_2}) - s(t;\boldsymbol{\alpha_1})|^2\, dt - \int |\tilde{s}(t;\boldsymbol{\alpha_1}) - s(t;\boldsymbol{\alpha_1})|^2\, dt\right)^2}{\int |\tilde{s}(t;\boldsymbol{\alpha_1}) - \tilde{s}(t;\boldsymbol{\alpha_1})|^2\, dt} \tag{3.23}$$

where $\boldsymbol{\alpha_1}$ and $\boldsymbol{\alpha_2}$ are two different data sequences. Also, $s(t)$ is the transmitted signal (exact CPM) and $\tilde{s}(t)$ is the PAM-based approximation of CPM which will be used at the receiver [31]. Just as with Euclidean distance, the minimum modified Euclidean distance among all possible data sequences gives an approximation of the probability of error and so (3.11) can be used to predict the BER curve, which prediction becomes increasingly accurate with increasing SNR [9, section 3.5.1].

Complexity

The complexity calculation is the same as ML PAM-based detection, but now there are R matched filter and R pseudo-symbols used in the filtering and multiplying, instead of P as in ML PAM-based detection. The only change comes in the calculation of the following:

$$\Phi = \sum_{i=0}^{R-1} 2^{\Theta_i}; \tag{3.24}$$

equations (3.19) and (3.20) still hold. Thus, the symbol-by-symbol detector requires fewer adds and multiplies and is also simpler in the fact that a MLSE is not required.

3.2.2 Reduced-Complexity Detection

Using an FM Limiter-Discriminator Detector

An FM limiter-discriminator detector simply removes the phase pulse train from the complex exponential and differentiates this pulse train, yielding the frequency pulse train. This pulse train is then fed into a matched filter matched to the frequency pulse. The matched-filter output is scaled and clipped. If the output sample at time $t = nT$ is positive, $\alpha(n) = 1$ is the decision; otherwise, a $\alpha(n) = 0$ is the decision. Analyis and complexity of this receiver will not be considered.

3.3 Application to EFTS

The following sections will describe in brief terms the modulator used as well as the various receivers in simulating an EFTS system.

3.3.1 CPM Modulator

The EFTS modulator is similar to other CPM modulators. A frequency pulse train is formed, and then pre-filtered by a Gaussian low-pass filter. The output of the filter is integrated and multiplied by $2\pi h$, which is input into a complex-exponential, thus forming the transmitted signal.

3.3.2 MLSE and Sub-Optimum Receivers

As discussed in Section 3.1, the MLSD uses matched filters to effect the recursive metric, whether the detector is complex-exponential-based or PAM-based. With weak CPM, the number of states is based solely on the number of symbol times spanned by the frequency pulse. Since EFTS uses a Gaussian low-pass filtered Manchester frequency pulse of length $2T$, there are only two states. The transition state always consists of one symbol and so there are two possible paths leaving and entering each state. The trellis is shown in Figure 3.1 where the states are labeled according to the cumulative metric found in (3.17).

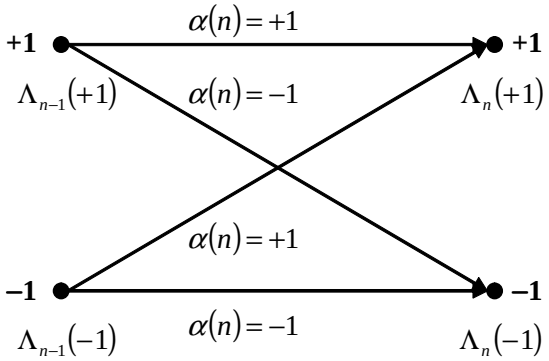

Figure 3.1: The two state trellis describing the signal state for the EFTS modulation.

Complex Exponential-based Detector In a complex exponential-based MLSD, the matched filters are matched to CPM signals for all possible data sequences. The matched filters only calculate the recursive metric ($\lambda_{m,i}$ found in (3.4)) and so only consider the current symbol time. In EFTS, the pulses span two symbol times and so, since the alphabet is binary and since only two symbols are transitioning in a symbol time, there are four possible waveforms in a given symbol time.

$$s(t) = \exp j\left(\pi h\left[\alpha(n)g(t-nT) + \alpha(n-1)g(t-(n-1)T)\right]\right) \tag{3.25}$$

where the four possibilities are found by varying $\alpha(n)$ and $\alpha(n-1)$ in $s(t)$. The MLSD detector is shown in Figure 3.2(a).

To calculate the metrics, simply replace $s(t;\tilde{\boldsymbol{\alpha}})$ found in (3.4) with the complex exponential found in (3.25) as follows:

$$\lambda_{m,i}(n;\tilde{\boldsymbol{\alpha}}_n) = \int_{nT}^{(n+1)T} r(t)\exp\left(j\pi h\left[\alpha(n)g(t-nT) + \alpha(n-1)g(t-(n-1)T)\right]\right)\,dt. \tag{3.26}$$

Also note that i and m found in this equation now both vary as $0 \leq i, m \leq 1$ since $L = 2$.

PAM-based Detector In a PAM-based MLSD, the matched filters are matched to the PAM pulses. The PAM-based MLSD is seen in Figure 3.2(b). Inside the MLSE block, the input to this block is multiplied by the possible pseudo-symbol combinations to find all of the metrics. It can be seen in this figure that the symbol-independent PAM pulse was completely neglected, yet the detector is still optimum. Verification of this metric as well as

the metric for the sub-optimum detector is easily done by applying the PAM decomposition to $s(t)$ in (3.3) and discarding terms that are constant with respect to $\tilde{\boldsymbol{\alpha}}$. The metrics for this MLSD are thus

$$\begin{aligned} \eta_k(n) &= \int_{-\infty}^{t} r(\tau) q_k(\tau)\, d\tau \Big|_{t=nT} \\ \lambda_{m,i}(n) &= \text{Re}\mathit{eft}\{\eta_0(n) d^*_{i,0}(n) + \eta_1(n) d^*_{i,1}(n)\}, \\ \text{and } \Lambda_j(n) &= \Lambda_i(n-1) + \sqrt{2E_b}\lambda_{m,i}(n). \end{aligned} \tag{3.27}$$

Symbol-by-symbol PAM-based Receiver In EFTS, there are only two symbol-dependent PAM pulses, as seen in (2.88) and (2.89). As the symbol-independent pulse carries no information, the only simplification that can be made is to remove $q_1(t)$, thus using the only pulse left, $q_0(t)$. Since $a_0(n) = J^{\alpha(n)}$, which is a function of the current symbol only, this simplification removes the need for a trellis; a symbol-by-symbol detector will suffice. This detector, which is sub-optimum, can be seen in Figure 3.2(c).

The metric for this detector is

$$\lambda(n) = \text{Re}\left\{ J^{-\alpha(n)} \int_{(n-1)T}^{nT} r(\tau) h_0(\tau)\, d\tau \right\}. \tag{3.28}$$

Clearly, there are only two possible metrics for each n since there are only two possible values that $\alpha(n)$ can take on. These two metrics are compared and the bit corresponding to the larger metric is taken as the likely transmitted symbol. Thus, the decision rule for this detector is

$$\hat{\alpha}(n) = \begin{cases} +1 & \text{Re}\left\{x_0(nT)e^{-j\pi h}\right\} \geq \text{Re}\left\{x_0(nT)e^{j\pi h}\right\} \\ -1 & \text{otherwise} \end{cases}. \tag{3.29}$$

Using $h = 50/3$, it is easy to show that the decision rule reduces to

$$\hat{\alpha}(n) = \begin{cases} +1 & \text{Im}\left\{x_0(nT)\right\} \geq 0 \\ -1 & \text{otherwise} \end{cases}. \tag{3.30}$$

3.3.3 FM Limiter-Discriminator

The FM limiter-discriminator can be built in several ways. In the simulations done for this work, the received signal, both in-phase and quadrature components, are ran

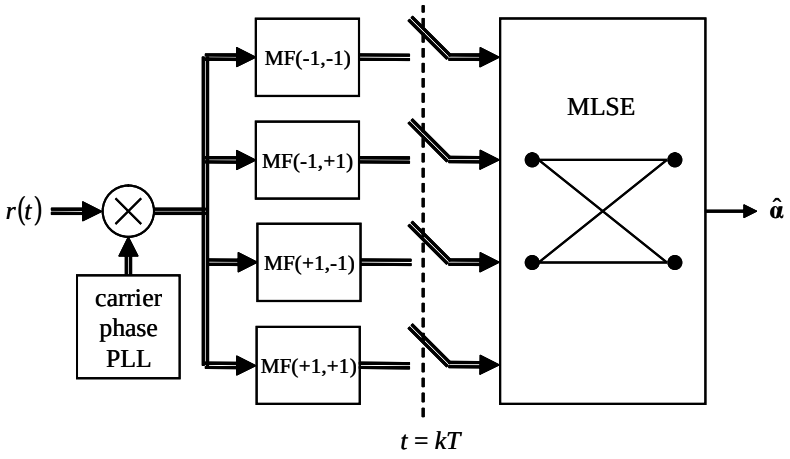

(a)

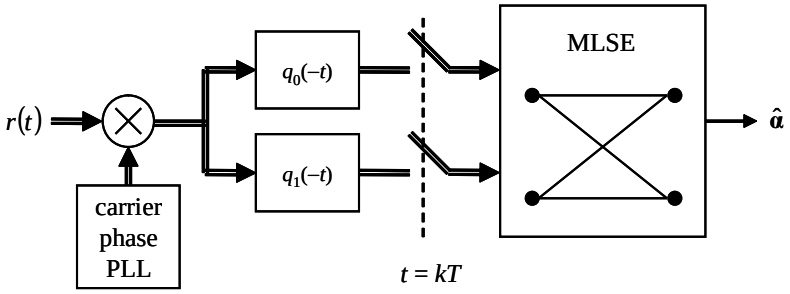

(b)

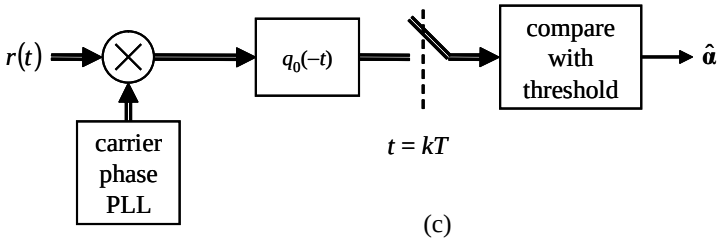

(c)

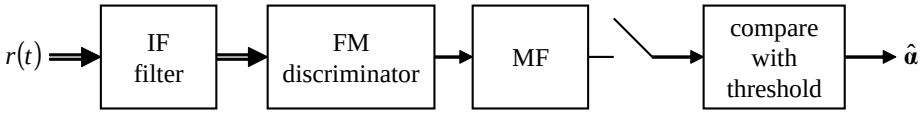

(d)

Figure 3.2: Coherent detectors for the EFTS modulation: (a) maximum likelihood detector based on the complex exponential representation; (b) maximum likelihood detector based on the PAM representation; (c) reduced-complexity detector based on the PAM representation; (d) non-coherent FM Limiter-Discriminator.

through intermediate frequency (IF) filters. These filters were modeled as 8^{th}-order Chebychev filters with peak ripple-widths of 0.5 dB and cutoff frequencies of $0.75F_s$ where F_s is the sample rate. After these filters, the derivative of each component is taken; the arctangent is then taken of the ratio of the filtered derivative of the quadrature component to the filtered derivative of the in-phase component. This result is divided by πh and clipped to be between ± 1. The result is compared to zero to determine whether a "1" was sent or a "0" was sent. This detector is shown in Figure 3.2(d).

3.4 EFTS Receiver Performance and Complexity

The performance of the PAM-based MLSD was approximately 5.62 dB better than an FM limiter-discriminator at 10^{-5} BER; the BER curves, with and without the symbol-independent pulse included as a matched filter, were for all intents and purposes identical. The performance of the symbol-by-symbol detector showed only a small loss of approximately 0.68 dB from optimal at a BER of 10^{-5}.

Distance analysis was performed in order to predict performance. Using (3.23), the following were found: $d^2_{\text{min}} \approx 1.18$ for the MLSD receiver and the mismatched distance $\tilde{d}^2_{\text{min}} \approx 1.02$ for the symbol-by-symbol receiver; for both receivers $W_{\text{min}} = 1$. The complexity for this case was calculated using (3.12), (3.13), (3.19), and (3.20). The simulation results and analysis for the MLSD receiver and the symbol-by-symbol receiver are compared in Figure 3.4 and the simulation results for all receivers are shown in Figure 3.5. The performance and complexity results are summarized in Table 3.1

The analyis and simulations were performed assuming an AWGN channel. EFTS applications are actually implemented in AWGN channels with added phase noise. Figure 3.3 shows the setup of the receiver simulations with phase noise and AWGN added. A fourth curve is seen in Figure 3.5 which shows how phase noise affects the simplified PAM-based receiver: still 4 dB better. (The FM limiter-discriminator was unaffected by the addition of phase noise.) For further explanation regarding the phase noise model, see Appendix B.

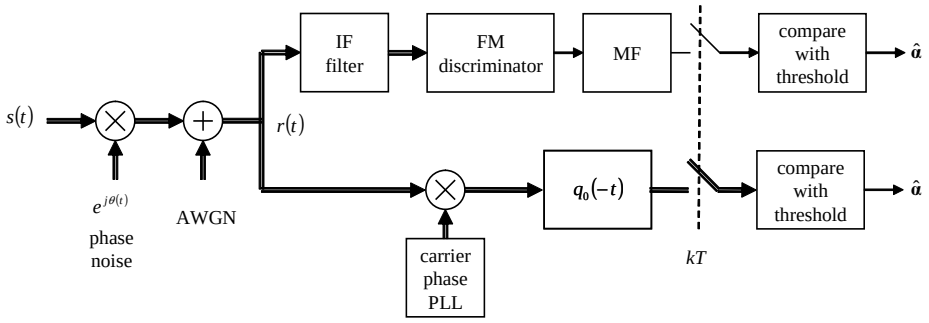

Figure 3.3: This figure shows the PAM-based simplified receiver and FM limiter-discriminator used to simulate operation in the presence of phase noise.

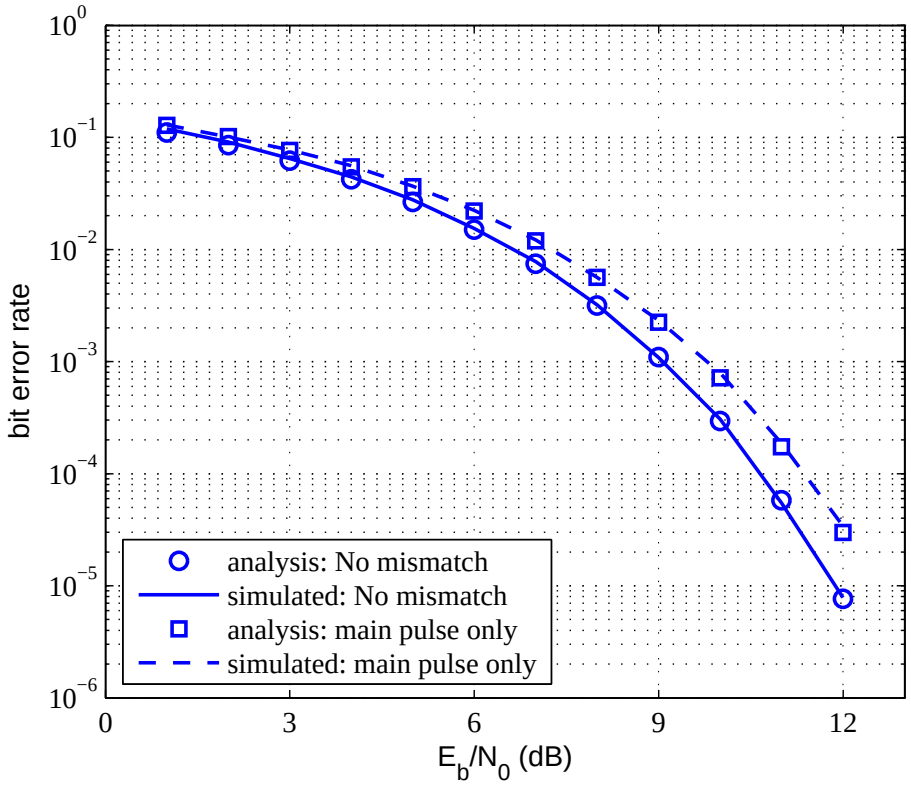

Figure 3.4: BER curves based on the Euclidean distance and the modified Euclidean distance anaylis, compared to the BER curves achieved from simulation. As can be seen, the analysis made an excellent prediction.

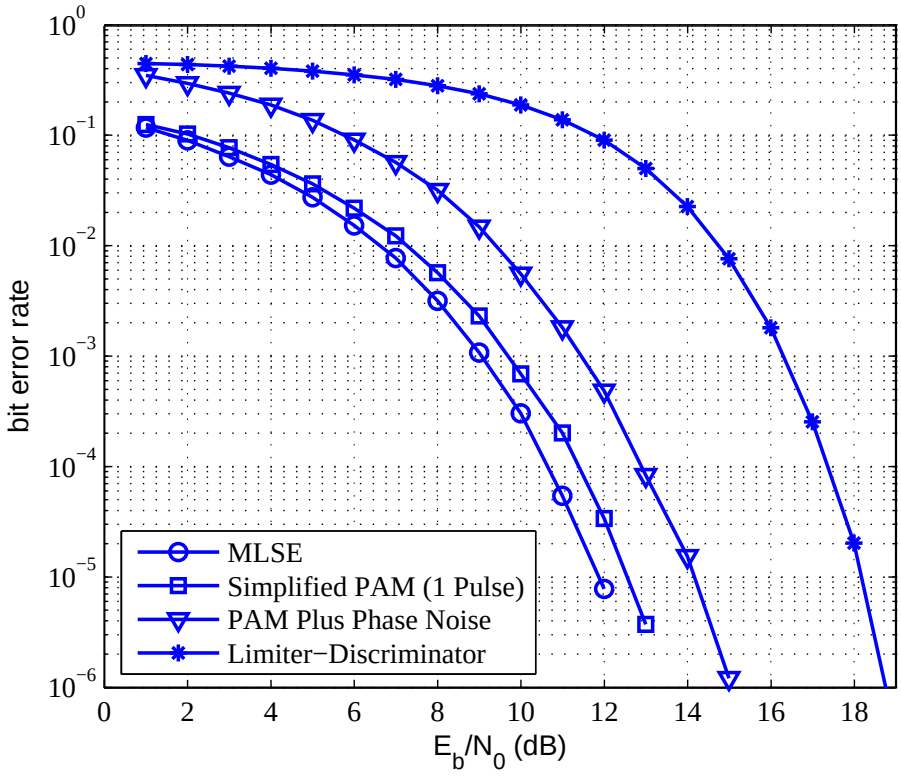

Figure 3.5: Bit error rate simulations for the three detection methods for the EFTS modulation, as well as the results for the phase noise simulation of the simplified PAM-based receiver.

Table 3.1: Comparison of the number of real-valued multiplies required by the three detectors illustrated in Figure 3.2.

Detector	E_b/N_0 for a BER of 10^{-5}	real multiples	real adds
ML-Complex Exponential	N/A	$8N$	$8N-4$
ML-PAM	11.6 dB	$6N+12$	6
Reduced-Complexity PAM	12.6 dB	$4N$	0
PAM With Phase Noise	14.2 dB	$4N$	0
FM Limiter-Discriminator	18.2 dB	N/A	N/A

Chapter 4

Conclusion

Although Laurent's work did not provide for a PAM representation of weak CPM, his work combined with the work of Mengali led to an approach for deriving a PAM representation for weak CPM. All the implications associated with a PAM decomposition were shown to apply to the PAM decomposition of weak CPM, most especially, the implication that a simplified receiver for the EFTS waveform could be constructed, based on this representation, that greatly outperforms a limiter-discriminator currently used in the EFTS system. The receiver performed with near optimal performance under the assumption of phase coherency and neatly outperformed the FM demodulator, even in the presence of phase noise present in EFTS applications.[1]

Another benefit of the PAM representation of weak CPM was the additional perspective given as to why weak CPM has poor performance. Namely, the PAM representation revealed a symbol-independent PAM pulse that is clearly wasted energy, accounting for the discrete lines observed in weak CPM as well as the small minimum distance exhibited by weak CPM. The PAM representation of weak CPM could be used to predict the energy in discrete lines due to the symbol-independent pulse.

[1] It may be that the effect of the phase noise could be lessened if h were chosen to be an odd multiple of $\frac{1}{2}$ bringing the two different complex-exponentials to an angle of $\pm\frac{1}{2}\pi$, and so making samples at time nT of the signal antipodal, thus maximizing the phase rotation necessary to cause an error due to the phase noise.

Appendix

Appendix A

Derivation of a PAM Decomposition of CPM and Weak CPM

A.1 CPM

The first order of business is to properly define the orginal CPM signal, from which the pulse-amplitude modulation (PAM) decomposition will be derived. The frequency pulse, $f(t)$, defines how the frequency of the signal changes during a given symbol period. It is well known that to find the phase of a signal, one must integrate the frequency over time; the frequency pulses will be assumed to integrate to $h\pi$. The following are some definitions that will be useful in the derivation of the PAM representation:

$$\begin{aligned} t &= NT + \tau \qquad 0 \leq \tau < T \\ J &= e^{jh\pi} \end{aligned} \tag{A.1}$$

Also

$$g(t) = \int_{-\infty}^{t} f(\tau) d\tau \tag{A.2}$$

where

$$g(t) = \begin{cases} 0 & t \leq 0 \\ \frac{1}{2} & t \geq LT \end{cases} . \tag{A.3}$$

A phase pulse that has reached its *terminal response*, has arrived in the time interval $t \geq LT$, whereas a phase pulse in the time interval $0 \leq t < LT$ is *transitioning*. (The behavior of $g(t)$ in this last time interval will not affect the discussion).

The following defines the CPM signal for $-\infty < t < (N+1)T$:

$$s(t) = \exp\left[j\theta_0 + 2\pi h \sum_{n=-\infty}^{N} \alpha(n) g(t-nT)\right]. \tag{A.4}$$

Assuming without loss of generality that θ_0 = 0,

$$s(t) = \exp\left[j2\pi h \sum_{n=-\infty}^{N-L} \alpha(n) g(t-nT)]\right] \cdot \exp\left[j2\pi h \sum_{n=N-L+1}^{N} \alpha(n) g(t-nT)\right]. \tag{A.5}$$

First $s(t)$ as found in (A.5) will be simplified. Consider $g(t-nT)$ for $n \geq N-L$. From (A.3),

$$g(t-nT) = \frac{1}{2} \qquad t - nT \geq LT. \tag{A.6}$$

From eq (A.1), $t = NT + \tau$ so

$$g(t-NT) = \frac{1}{2} \qquad (N-n)T + \tau \geq LT \tag{A.7}$$

or

$$g(t-nT) = \frac{1}{2} \qquad nT \leq (N-L)T + \tau. \tag{A.8}$$

And since $0 \leq \tau < T$,

$$g(t-nT) = \frac{1}{2} \qquad n \leq N-L. \tag{A.9}$$

In words, $g(t-nT)$ will have reached its terminal response for $n \leq N-L$. Thus, the terms in the first sum of (A.5) are all simply $\alpha(n)h\pi$:

$$s(t) = \exp\left[j \sum_{n=-\infty}^{N-L} \alpha(n)\pi h\right] \cdot \exp\left[j2\pi h \sum_{n=N-L+1}^{N} \alpha(n) g(t-nT)\right], \tag{A.10}$$

which can be rewritten as

$$\begin{aligned} s(t) &= J^{\sum_{n=-\infty}^{(N-L)} \alpha(n)\pi h} \cdot \exp\left[j2\pi h \sum_{n=N-L+1}^{N} \alpha(n) g(t-nT)\right] \\ &= J^{\sum_{n=-\infty}^{(N-L)} \alpha(n)\pi h} \prod_{i=0}^{L-1} \exp\left[j2\pi h \cdot \alpha(N-i) g(t-(N-i)T)\right]. \end{aligned} \tag{A.11}$$

Next it will be shown that

$$\exp[j2\pi h\alpha(n)g(t-NT)] = u(t+[L-N]T) + J^{\alpha(n)}u(t-NT). \tag{A.12}$$

In the process, $u(t)$ will be defined. (In the following derivation $2\pi h \cdot g(t-NT)$ will be represented simply by g and $\alpha(n)$ by α.) First, from Euler's identity

$$\exp[j\alpha g] = \cos(\alpha g) + j\sin(\alpha g). \tag{A.13}$$

Since $\alpha \in \pm 1$, it just affects the sign of the argument of the sine and cosine functions, and since cosine is an even function and sine is an odd function. Thus, the complex exponential can be rewritten as:

$$\exp[j\alpha g] = \cos g + j\alpha \sin g. \tag{A.14}$$

This next step is in the dark; the reasoning for it will become apparent

$$\begin{aligned}\exp[j\alpha g] &= \frac{\sin(\pi h)\cos g}{\sin(\pi h)} + j\alpha\frac{\sin(\pi h)\sin g}{\sin(\pi h)} \\ &= \frac{\sin(\pi h)\cos g}{\sin(\pi h)} + j\alpha\frac{\sin(\pi h)\sin g}{\sin(\pi h)} - \frac{\cos(\pi h)\sin g}{\sin(\pi h)} + \frac{\cos(\pi h)\sin g}{\sin(\pi h)}\end{aligned} \tag{A.15}$$

Combining the first and third terms and factoring out the common $\sin \pi hg$ in the second and fourth terms gives

$$\exp[j\alpha g] = \frac{\sin(\pi h - g)}{\sin(\pi h)} + \frac{\sin g \cdot [\cos(\pi h) + j\alpha\sin(\pi h)]}{\sin(\pi h)}. \tag{A.16}$$

Inserting α into the cosine of the second term and pushing the α back inside the sine, also of the second term, yields:

$$\exp[j\alpha g] = \frac{\sin(\pi h - g)}{\sin(\pi h)} + \frac{\sin g \cdot [\cos(\alpha\pi h) + j\sin(\alpha\pi h)]}{\sin(\pi h)} \tag{A.17}$$

The right hand side of the numerator of the second term is easily recognizable as the expanded form of a complex exponential:

$$\begin{aligned}\exp[j\pi h\alpha g] &= \frac{\sin(\pi h - g)}{\sin(\pi h)} + \frac{\sin g \cdot \exp[j\alpha\pi h]}{\sin(\pi h)} \\ &= \frac{\sin(\pi h - g)}{\sin(\pi h)} + J^{\alpha\pi h}\frac{\sin g}{\sin(\pi h)}.\end{aligned} \tag{A.18}$$

Now define a function to be the argument of the sine in the numerator of the first term of (A.18) during one interval. Let the same function equal the argument of the sine in the numerator of the second term during another interval disjoint from the first:

$$\Psi(t) = \begin{cases} 2\pi hg(t) & for\ t < LT \\ \pi h - 2\pi hg(t - LT) & for\ t \geq LT \end{cases} \tag{A.19}$$

$$u(t) = \frac{\sin[\Psi(t)]}{\sin(\pi h)}. \tag{A.20}$$

Thus

$$u(t + [L - N]T) = \frac{\sin[\Psi(\tau + NT + (L - N)T)]}{\sin(\pi h)} \tag{A.21}$$

$$= \frac{\sin[\Psi(\tau + LT)]}{\sin(\pi h)}. \tag{A.22}$$

Also note that $0 \leq \tau < T$. It is clear that $\tau + LT \geq LT$. Thus

(A.23)

$$u(t + [L - N]T) = \frac{\sin[\pi h - 2\pi hg(t - LT)]}{\sin(\pi h)}. \tag{A.24}$$

Following a similar path it is easy to see that

$$u(t - NT) = \frac{\sin\ 2\pi hg(t - NT)}{\sin(\pi h)}. \tag{A.25}$$

Combining the latter equation with (A.18)

$$\exp[j\pi h\alpha(n)g(t - nT)] = u(t + [L - n]T) + J^{\alpha(n)}u(t - nT). \tag{A.26}$$

This is the identity needed to form Laurent's PAM representation of CPM. Using this identity with (A.11)

$$s(t) = J^{\sum_{n=-\infty}^{(N-L)} \alpha(n)} \prod_{i=0}^{L-1} [u(t + [i + L - N]T) + J^{\alpha(N-i)}u(t + [i - N]T)]. \tag{A.27}$$

Example for $L = 2$ Part 6

Consider the case $N = 0$ (i.e., the time interval $0 < t < T$). Expanding the product in (A.30)

$$\begin{aligned} p &= \prod_{i=0}^{1} [u(t + [i+2]T) + J^{\alpha(-i)} u(t + iT)] \\ &= [u(t+2T) + J^{\alpha(0)} u(t)] \cdot [u(t+3T) + J^{\alpha(-1)} u(t+T)] \\ &= u(t+2T)u(t+3T) + J^{\alpha(-1)} u(t+T)u(t+2T) \\ &\quad + J^{\alpha(0)} u(t)u(t+3T) + J^{\alpha(0)+\alpha(-1)} u(t)u(t+T). \end{aligned} \tag{A.28}$$

Define $C_0(t) = u(t)u(t+T)$. Thus

$$u(t+T)u(t+2T) = C_0(t+T). \tag{A.29}$$

Also define $C_1(t) = u(t)u(t+3T)$. And so for $0 < t < T$

$$s(t) = J^{\sum_{n=-\infty}^{-2} \alpha(n)} \cdot [C_0(t+2T) + J^{\alpha(-1)} C_0(t+T) + J^{\alpha(0)+\alpha(-1)} C_0(t) + J^{\alpha(0)} C_1(t)]. \tag{A.30}$$

For $T < t < 2T$,

$$\begin{aligned} p &= \prod_{i=0}^{1} [u(t + [i+2-1]T) + J^{\alpha(1-i)} u(t + [i-1]T)] \\ &= [u(t+T) + J^{\alpha(1)} u(t-T)] \cdot [u(t+2T) + J^{\alpha(0)} u(t)] \\ &= u(t+T)u(t+2T) + J^{\alpha(0)} u(t)u(t+T) + J^{\alpha(1)} u(t-T)u(t+2T) \\ &\quad + J^{\alpha(1)+\alpha(0)} u(t-T)u(t). \end{aligned} \tag{A.31}$$

Thus for $T < t < 2T$,

$$\begin{aligned} s(t) &= J^{\sum_{n=-\infty}^{-1} \alpha(n)} \cdot [C_0(t+T) + J^{\alpha(0)} C_0(t) \\ &\qquad + J^{\alpha(1)+\alpha(0)} C_0(t-T) + J^{\alpha(1)} C_1(t-T)] \\ s(t) &= J^{\sum_{n=-\infty}^{-2} \alpha(n)} \cdot [J^{\alpha(-1)} C_0(t+T) + J^{\alpha_0+\alpha(-1)} C_0(t) \\ &\qquad + J^{\alpha_1+\alpha_0+\alpha(-1)} C_0(t-T) + J^{\alpha_1+\alpha(-1)} C_1(t-T)]. \end{aligned} \tag{A.32}$$

And for $2T < t < 3T$,

$$\begin{aligned} p &= \prod_{i=0}^{1}[u(t+[i+2-2]T) + J^{\alpha(2-i)}u(t+(i-2)T] \\ &= [u(t) + J^{\alpha(2)}u(t-2T)] \cdot [u(t+T) + J^{\alpha(1)}u(t-T)] \\ &= u(t)u(t+T) + J^{\alpha(1)}u(t-T)u(t) + J^{\alpha(2)}u(t-2T)u(t+T) \\ &\quad + J^{\alpha(2)+\alpha(1)}u(t-2T)u(t-T). \end{aligned} \tag{A.33}$$

Thus for $2T < t < 3T$,

$$\begin{aligned} s(t) &= J^{\sum_{n=-\infty}^{0}\alpha(n)} \cdot [C_0(t) + J^{\alpha(1)}C_0(t-T) \\ &\qquad + J^{\alpha(2)+\alpha(1)}C_0(t-2T) + J^{\alpha(2)}C_1(t-2T)] \\ &= J^{\sum_{n=-\infty}^{-2}\alpha(n)} \cdot [J^{\alpha_0+\alpha(-1)}C_0(t) + J^{\alpha_1+\alpha_0+\alpha(-1)}C_0(t-T) \\ &\qquad + J^{\alpha_2+\alpha_1+\alpha_0+\alpha(-1)}C_0(t-2T) + J^{\alpha_2+\alpha_0+\alpha(-1)}C_1(t-2T)] \end{aligned} \tag{A.34}$$

To summarize, the equations for N = 0,1,2, can be rewritten, as:

$$\begin{aligned} 0 < t < T: \quad & s(t) = J^{\sum_{n=-\infty}^{-2}\alpha(n)} \cdot [C_0(t+2T) + J^{\alpha(-1)}C_0(t+T) + J^{\alpha(0)+\alpha(-1)}C_0(t) + J^{\alpha(0)}C_1(t)] \\ T < t < 2T: \quad & s(t) = J^{\sum_{n=-\infty}^{-2}\alpha(n)} \cdot [J^{\alpha(-1)}C_0(t+T) + J^{\alpha_0+\alpha(-1)}C_0(t) \\ & \qquad + J^{\alpha_1+\alpha_0+\alpha(-1)}C_0(t-T) + J^{\alpha_1+\alpha(-1)}C_1(t-T)] \\ 2T < t < 3T: \quad & s(t) = J^{\sum_{n=-\infty}^{-2}\alpha(n)} \cdot [J^{\alpha_0+\alpha(-1)}C_0(t) + J^{\alpha_1+\alpha_0+\alpha(-1)}C_0(t-T) \\ & \qquad + J^{\alpha_2+\alpha_1+\alpha_0+\alpha(-1)}C_0(t-2T) + J^{\alpha_2+\alpha_0+\alpha(-1)}C_1(t-2T)]. \end{aligned} \tag{A.35}$$

Note that the coefficents of the C_K terms are the same for each shifted version of $C_K(t)$. For example, the coefficient for $C_0(t)$ is always $J^{\alpha_0+\alpha(-1)}$. Laurent saw this pattern and realized that the equations (A.30), (A.32), and (A.34) could be combined to form, for $0 < t < 3T$,

$$\begin{aligned} s(t) = J^{\sum_{n=-\infty}^{-2}\alpha(n)} \cdot [&C_0(t+2T) + J^{\alpha(-1)}C_0(t+T) + J^{\alpha(0)+\alpha(-1)}C_0(t) \\ &+ J^{\alpha_1+\alpha_0+\alpha(-1)} + C_0(t-T) + J^{\alpha_2+\alpha_1+\alpha_0+\alpha(-1)}C_0(t-2T) \\ &+ J^{\alpha_2+\alpha_0+\alpha(-1)}C_1(t-2T) + J^{\alpha_1+\alpha(-1)}C_1(t-T) + J^{\alpha(0)}C_1(t)]. \end{aligned} \tag{A.36}$$

which holds for $0 < t < 3T$. This expression can be expanded to include all time, yielding Laurent's result for $L = 2$. If the same process is done for other values of L, Laurent's final result is found:

$$s(t) = \sum_{N=-\infty}^{\infty} \sum_{K=0}^{2^{L-1}-1} J^{A_K(N)} C_K(t - nT) \tag{A.37}$$

where

$$A_K(N) = \sum_{n=-\infty}^{N} \alpha(n) - \sum_{i=1}^{L-1} \alpha(N-i) \cdot \beta_K(i) \tag{A.38}$$

and $\beta_K(i)$ is the i-th coefficient for the radix-2 decomposition of an integer K, as seen in the following:

$$K = \sum_{i=1}^{L-1} 2^{i-1} \cdot \beta_K(i). \tag{A.39}$$

The PAM pulses are time-limited according to the following set of equations:

$$C_0 \neq 0 \qquad 0 < t < (L+1)T \tag{A.40}$$

$$C_1 \neq 0 \qquad 0 < t < (L-1)T \tag{A.41}$$

$$C_2, C_3 \neq 0 \qquad 0 < t < (L-2)T \tag{A.42}$$

$$C_4, C_5, C_6, C_7 \neq 0 \qquad 0 < t < (L-3)T \tag{A.43}$$

$$\vdots \tag{A.44}$$

$$C_{2^{L-1}/2}, \ldots, C_{2^{L-1}-1} \neq 0 \qquad 0 < t < T. \tag{A.45}$$

This allows correlatation of our CPM signal with the outputs of two filters based on C_0 and C_1. Then after multiplying the output by the possible symbol combinations, the Viterbi algorithm can be used to decode the most likely sequence of symbols. This would not be possible if an expression for $s(t)$ could not be found that was valid for all N. For example, if the combination of symbols that multiply $C_0(t - T)$ differed from the N=2 case to the N=3 case, the filter approach could not be used.

A.2 Weak CPM

If $g(t)$ is redefined for weak CPM, i.e.

$$g(t) = 0 \qquad t \leq 0,\ t \geq LT, \tag{A.46}$$

the terms in the first sum of (A.30) equal to $\alpha(n) \cdot 0$, altering it as shown here for three values of N:

$$0 < t < T: \quad s(t) = [C_0(t+2T) + J^{\alpha(-1)}C_0(t+T) + J^{\alpha(0)+\alpha(-1)}C_0(t) + J^{\alpha(0)}C_1(t)] \tag{A.47}$$

$$T < t < 2T: \quad s(t) = [C_0(t+T) + J^{\alpha(0)}C_0(t) + J^{\alpha(1)+\alpha(0)}C_0(t-T) + J^{\alpha(1)}C_1(t-T)] \tag{A.48}$$

$$2T < t < 3T: \quad s(t) = [C_0(t) + J^{\alpha(1)}C_0(t-T) + J^{\alpha(2)+\alpha(1)}C_0(t-2T) + J^{\alpha(2)}C_1(t-2T)]. \tag{A.49}$$

Now in this case, unlike generic CPM, the coefficients of the C_K terms change with each time step. For example, consider again $C_0(t)$. When $N = 0$, $C_0(t)$ has a coefficient of $J^{\alpha(0)+\alpha(-1)}$; at $N = 1$, this coefficient becomes $J^{\alpha(0)}$. This makes it impossible, using this form, to create a linear expression for $s(t)$ for all N. Thus, Laurent's PAM approach applied to weak CPM does not yield a linear result, and so another approach must be taken to find a linear PAM representation of weak CPM.

A.3 Pulses That are Zero: the Full Derivation

Consider the definition of a frequency pulse, $f(t)$, of length LT, that integrates to zero:

$$\begin{aligned} f(t) &> 0 \quad 0 < t < \kappa LT \\ f(t) &< 0 \quad \kappa LT < t < LT, \end{aligned} \tag{A.50}$$

where $0 < \kappa < 1$. Referring to (A.50) it is seen that $f^+(t)$, which integrates to A, is zero for $\kappa LT < t < LT$, and $f^-(t)$, which integrates to -A, is zero for $0 < t < \kappa LT$. $g^+(t)$ and $g^-(t)$ thus become:

$$g^+(t) = \begin{cases} 0 & t < 0 \\ A & t > \kappa LT \end{cases} \tag{A.51}$$

$$g^-(t) = \begin{cases} 0 & t < \kappa LT \\ -A & t > LT \end{cases}. \tag{A.52}$$

(A.53)

With $g^+(t)$ and $g^-(t)$ in hand, $\Psi^+(t)$ and $\Psi^-(t)$ can both be determined as well as $u^+(t)$ and $u^-(t)$. It is in this determination that it can be seen that some PAM pulses are zero. $\Psi^+(t)$ and $\Psi^-(t)$ are calculated as follows:

$$\Psi^+(t) = \begin{cases} g^+(t) & 0 < t < LT \\ A - g^+(t) & LT < t < 2LT \end{cases} \tag{A.54}$$

and

$$\Psi^-(t) = \begin{cases} -g^-(t) & 0 < t < LT \\ A + g^-(t) & LT < t < 2LT \end{cases}. \tag{A.55}$$

(Since $D_K(t)$ was defined using $-g^-(t)$, $\Psi^-(t)$ also uses $-g^-(t)$ in its definition.) For a given set of PAM pulses, $u(t)$ is a function of $\Psi(t)$ (see (2.6)); thus $u^+(t)$ and $u^-(t)$ can be defined as:

$$\begin{aligned} u^+(t) &\neq 0 \quad 0 < t < (\kappa L + L)T \\ u^-(t) &\neq 0 \quad \kappa LT < t < 2LT, \end{aligned} \tag{A.56}$$

where $u^+(t)$ is based on $\Psi^+(t)$ and $u^-(t)$ is based on $\Psi^-(t)$.

Example for $L = 2$ Part 7

Consider once again the example for $L = 2$, where at this point the products of shifted versions of $u^+(t)$ and $u^-(t)$ are used to find PAM pulses that are zero. Recall (2.36):

$$\begin{aligned} s(t) =& [C_0(t)D_0(t) + C_1(t)D_1(t)] \\ &+ J^{\alpha(-1)}C_0(t)D_1(t) \\ &+ J^{\alpha(0)}[C_0(t)D_0(t+T) + C_1(t)D_0(t+2T)] \\ &+ J^{\alpha(0)+\alpha(-1)}C_0(t)D_0(t+2T) \\ &+ J^{-\alpha(-1)}C_1(t)D_0(t) \\ &+ J^{\alpha(0)-\alpha(-1)}C_1(t)D_0(t+T) \\ &+ J^{-\alpha(0)}[C_0(t+T)D_0(t) + C_0(t+T)D_1(t)] \\ &+ J^{-\alpha(0)+\alpha(-1)}C_0(t+T)D_1(t) \\ &+ J^{-\alpha(0)-\alpha(-1)}C_0(t+2T)D_0(t). \end{aligned} \tag{A.57}$$

In order to determine which pulses are zero, the interval to which each of the PAM-pulse products is time-limited will be considered.

PAM pulse lengths First, the interval to which each of the $C_K(t)$ and $D_K(t)$ pulses is time-limited must be considered. The length of each $C_K(t)$ and $D_K(t)$ can be calculated by examing the definition of $C_K(t)$, found in (2.5) (repeated here for convenience), combined with the definition of $u(t)$ as found in (A.56).

$$\begin{aligned} C_K(t) &= \prod_{i=0}^{L-1} u(t + [i + \beta_K(i)L]T) \\ K &= \sum_{i=1}^{L-1} 2^{i-1} \cdot \beta_K(i) \end{aligned} \tag{A.58}$$

For general L, consider the intervals to which $C_K(t)$ and $D_K(t)$ are time-limited:

$$C_0 \neq 0 \qquad 0 < t < (\kappa L + 1)T \tag{A.59}$$

$$D_0 \neq 0 \qquad \kappa LT < t < (L+1)T \tag{A.60}$$

$$C_1 \neq 0 \qquad 0 < t < (\kappa L - 1)T \tag{A.61}$$

$$D_1 \neq 0 \qquad \kappa LT < t < (L-1)T \tag{A.62}$$

$$C_2, C_3 \neq 0 \qquad 0 < t < (\kappa L - 2)T \tag{A.63}$$

$$D_2, D_3 \neq 0 \qquad \kappa LT < t < (L-2)T \tag{A.64}$$

$$C_4, C_5, C_6, C_7 \neq 0 \qquad 0 < t < (\kappa L - 3)T \tag{A.65}$$

$$D_4, D_5, D_6, D_7 \neq 0 \qquad \kappa LT < t < (L-3)T \tag{A.66}$$

$$\vdots \tag{A.67}$$

$$C_{2^{L-1}/2}, \ldots, C_{2^{L-1}-1} \neq 0 \qquad 0 < t < (\kappa L - (L-1))T \tag{A.68}$$

$$D_{2^{L-1}/2}, \ldots, D_{2^{L-1}-1} \neq 0 \qquad \kappa LT < t < (L - (L-1))T \tag{A.69}$$

All pulses with $K > 0$ are time-limited to intervals that can be expressed in the form $0 < t < (\kappa L - R)T$ or $\kappa LT < t < (L - R)T$, where R is an integer. Those pulses defined with the former interval are zero for $\kappa \leq \frac{R}{L}$ whereas the pulses defined with the latter interval are zero for $\kappa \geq 1 - \frac{R}{L}$. Thus as K increases, an increasing number of PAM pulses are zero for an increasing range of values of κ. This can greatly simplify the PAM representation.

Example for $L = 2$ Part 8

Consider an example where $L = 2$ and a general weak phase pulse. $C_0(t)$ is the product of $u(t)$ and $u(t+T)$. $u(t)$ is time-limited to $0 < t < 4T$. Thus, $C_0(t)$ has a length of $3T$. $C_1(t)$ is the product of $u(t)$ and $u(t+3T)$ and thus has a length of T.

Now replace the general weak phase pulse with with a weak phase pulse as defined in (2.15). Using (A.56), $u^+(t)$ is found to be time-limited to $0 < t < (2\kappa + 2)T$ and $u^-(t)$ is time-limited to $2\kappa T < t < 4T$. This alters the interval to which C_0 and D_0 are time-limited:

$$\begin{aligned} C_0 &\neq 0 \qquad 0 < t < (2\kappa + 1)T \\ D_0 &\neq 0 \qquad 2\kappa T < t < 3T. \end{aligned} \tag{A.70}$$

Also,

$$\begin{aligned} C_1 &\neq 0 \qquad 0 < t < (2\kappa - 1)T \\ D_1 &\neq 0 \qquad 2\kappa < t < T. \end{aligned} \tag{A.71}$$

The results in (A.70) and (A.71) reduce the number of pulses in (2.36)) to 4:

$$\begin{aligned} C_0(t)D_0(t+T) + C_1(t)D_0(t+2T) \neq 0 \qquad & \max[0,(2\kappa-1)T] < t < \min[(2\kappa+1)T, 2T \\ C_0(t)D_0(t+2T) \neq 0 \qquad & 0 < t < T \\ C_0(t)D_0(t) + C_1(t)D_1(t) \neq 0 \qquad & 2\kappa T < t < (2\kappa+1)T \\ C_0(t)D_1(t) \neq 0 \qquad & 2\kappa T < t < T. \end{aligned} \tag{A.72}$$

Thus the final PAM pulses for this special case of weak CPM are as follows:

$$\begin{aligned} q_0(t) &= C_0(t)D_0(t+T) + C_1(t)D_0(t+2T) \\ q_1(t) &= C_0(t)D_0(t+2T) \\ q_2(t) &= C_0(t)D_1(t) \\ q_3(t) &= C_0(t)D_0(t) + C_1(t)D_1(t). \end{aligned} \tag{A.73}$$

It can be seen from (2.36) that the psuedo-symbols corresponding to the PAM pulses in (A.73) are

$$\begin{aligned} a_0(n) &= J^{\alpha(n)} \\ a_1(n) &= J^{\alpha(n)+\alpha(n-1)} \\ a_2(n) &= J^{\alpha(n-1)} \\ a_3(n) &= J^0 = 1. \end{aligned} \tag{A.74}$$

Appendix B

Phase Noise and Phase-Lock Loop Models

The phase noise that is being simulated is due to the large amounts of vibrations found experimentally to be present in flight vehicles using the EFTS. It was estimated that the phase noise had an RMS frequency deviation of 4 kHz and an equivalent noise bandwidth of 2.5 kHz [8]. The simulations were done in discrete-time with a sample rate of

$$N = \frac{F_s}{R_b} = 56\frac{\text{Samples}}{\text{Bit}}. \tag{B.1}$$

The following simple recursive filter, where a was chosen so that the phase noise had the desired RMS frequency deviation and equivalent noise bandwidth,

$$F_{\text{PN}}(z) = \frac{1}{1 + az^{-1}}, \tag{B.2}$$

was used to generate the phase noise as

$$\rho(n) = f_{\text{PN}}(n) \star z(n) \tag{B.3}$$

where $\star$ denotes convolution. Also, $f_{\text{PN}}(n)$ is the time-domain version of the filter in (B.2), $\rho(n)$ is the simulated frequency noise, and $z(n)$ is white Gaussian noise. The variance of $z(n)$, σ_z^2 as well as a can be calculated based on the target equivalent noise bandwidth in radians, ω_{NB}, and the target RMS frequency deviation in radians, σ^2_{RMS}, of the noise, using the following equations:

$$a = \frac{2\omega_{\text{NB}} - 1}{2\omega_{\text{NB}} - 1} \tag{B.4}$$

$$\sigma_z^2 = |a^2 - 1|\sigma^2_{\text{RMS}}. \tag{B.5}$$

Figure B.1 shows the setup of the noise generator.

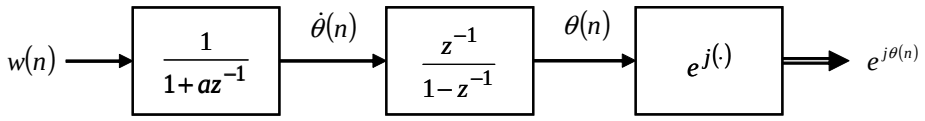

Figure B.1: This figure shows the simulation setup used to generate phase noise, which generator is injected with white Gaussian noise ($w(n)$).

The filter output was then sent through an integrator to turn the noise into phase noise, which noise was then added to the phase of the signal as follows:

$$r(n) = s(n)e^{jp(n)} + w(n) \tag{B.6}$$

with

$$p(n) = T_s \sum \rho(n) \tag{B.7}$$

where $w(n)$ is AWGN.

The simulation in a simple AWGN channel assumed ideal phase coherency, so a phase-lock loop (PLL) was not actually built into the simulation. A PLL must be included to simulte the effect of PLL tracking errors in the presence of phase noise.

The phase noise was added to the phase of the received signal as previously noted. The phase noise was also filtered by a filter that was equivalent to the frequency response of a PLL, in order to simulate the effect a PLL would have on the phase noise. The PLL was chosen to have a damping factor, $\zeta = 1$, and a noise-bandwidth, $B_n = 18$. The following equation was used for the equivalent transfer function of the PLL:

$$F_{\text{PLL}}(z) = \frac{(K_1 + K_2)z^{-1} - K_1 z^{-2}}{1 + (K_1 + K_2 - 2)z^{-1} + (1 - K_1)z^{-2}} \tag{B.8}$$

with

$$K_1 = \frac{\frac{4\zeta}{N}\left(\frac{B_n T_b}{\zeta + \frac{1}{4\zeta}}\right)}{1 + \frac{2\zeta}{N}\left(\frac{B_n T_b}{\zeta + \frac{1}{4\zeta}}\right) + \left(\frac{B_n T_b}{N\left(\zeta + \frac{1}{4\zeta}\right)}\right)^2} \tag{B.9}$$

$$K_2 = \frac{\frac{4}{N^2}\left(\frac{B_n T_b}{\zeta + \frac{1}{4\zeta}}\right)^2}{1 + \frac{2\zeta}{N}\left(\frac{B_n T_b}{\zeta + \frac{1}{4\zeta}}\right) + \left(\frac{B_n T_b}{N\left(\zeta + \frac{1}{4\zeta}\right)}\right)^2} \tag{B.10}$$

where N is the number of samples per bit used in the simulation and $T_b = \frac{1}{R_b}$ is the bit time.

The phase noise could be added to the phase of the received signal, as well as filtered by the PLL-equivalent filter, the results of which being subtracted off the phase of the signal, all before the signal is matched-filtered. However, in this configuration, the noise bandwidth of the PLL could be cranked up to eliminate the phase noise altogether. Therefore, after the phase noise was added to the received signal but before it was filtered by the PLL, it was modified by adding the quadrature component of the AWGN ($w(n)$ in (B.6)) in order to get a more realistic result as shown in the following equation:

$$\tilde{p}(n) = (p(n) + w_Q(n)) \star f_{\text{PLL}}(n) \tag{B.11}$$

where $f_{\text{PLL}}(n)$ is the time-domain version of the filter in (B.8) and $w_Q(n) = \text{Im}\{w(n)\}$. Thus the filtered phase noise will cancel some of the phase noise, simulating the imperfect yet still effective operation of a PLL through the following equation:

$$r(n) = s(n)e^{jp(n)}e^{-j\tilde{p}}(n) + w(n). \tag{B.12}$$

It should be noted that all of this assumes a priori that a PLL could be designed that functions in the presence of such severe phase noise as that found in EFTS applications.

Bibliography

[1] S. Cronk, M. Tobin, and R. Sakahara, "Enhanced flight termination system study overview and status," in *Proceedings of the International Telemetering Conference*, (Las Vegas, NV), pp. 397–403, October 2001.

[2] Range Safety Group, *IRIG Standard 319-99: Flight Termination Systems Commonality Standard*. Range Commanders Council, U. S. Army White Sands Missile Range, New Mexico, 1999.

[3] Range Safety Group, *IRIG Standard 208-85: IRIG Standards for UHF Command Systems*. Range Commanders Council, U. S. Army White Sands Missile Range, New Mexico, 1985.

[4] Range Safety Group, *Document 307-79: Range Safety Transmitting Systems 406 – 549 MHz Band*. Range Commanders Council, U. S. Army White Sands Missile Range, New Mexico, 1979.

[5] Directorate of Safety, Vandenberg AFB, California, *Eastern and Western Range Regulation (EWRR) 127-1 Range Safety Requirements*, 1985. (This document was formerly known as WSMCR 127-1 and EWR 127-1 and will be replaced by a HQ AFSPC developed publication, AFSPCMAN 91-970, *Range Safety User Requirements Manual*, released by the Federal Aviation Administration in the near future.).

[6] D. Arce, R. Garza, and T. McAndrews, "Enhanced flight termination study — phase II and III status," in *Proceedings of the International Telemetering Conference*, (Las Vegas), pp. 84–89, October 2001.

[7] T. McAndrews, "Enhanced flight termination system program — part two," in *Proceedings of the International Telemetering Conference*, (San Diego, CA), pp. 748 – 753, October 2002.

[8] E. Law, 2002. private communication.

[9] J. B. Anderson, T. Aulin, and C.-E. Sundberg, *Digital Phase Modulation*. 233 Spring Street, New York, NY 10013: Plenum Press, 1986.

[10] P. A. Laurent, "Exact and approximate construction of digital phase modulations by superposition of amplitude modulated pulses," *IEEE Transactions on Communications*, vol. 34, pp. 150–160, February 1986.

[11] U. Mengali and M. Morelli, "Decomposition of M-ary CPM signals into PAM waveforms," *IEEE Transactions on Information Theory*, vol. 41, pp. 1265–1273, September 1995.

[12] X. Huang and Y. Li, "The PAM Decomposition of CPM signals With Integer Modulation Index," *IEEE Transactions on Communications*, vol. 51, pp. 543–546, April 2003.

[13] E. Perrins and M. Rice, "PAM decomposition of M-ary multi-h CPM." to appear in *IEEE Transactions on Communications*, 2005.

[14] J. Zhang, N. Chi, P. Holm-Nielsen, C. Peucheret, and P. Jeppesen, "Performance of Manchester-coded payload in an optical FSK labeling scheme," *IEEE Phtonics Tehcnology Letters*, vol. 15, pp. 1174–1176, August 2003.

[15] P. Hooijmans, M. Tomesen, and A. Van de Grijp, "Penalty free biphase linecoding for pattern independent FSK coherent transmission systems," *IEEE Journal of Lightwave Technology*, vol. 8, pp. 323–328, March 1990.

[16] C. Tan, T. Tjhung, and H. Singh, "Performance of narrow-band Manchester coded FSK with discriminator detection," *IEEE Transactions on Communications*, vol. 31, pp. 659–667, May 1983.

[17] C. Tan, T. Tjhung, and H. Singh, "Error rates for narrowband Manchester coded digital FM," in *Proceedings of the IEEE National Telecommmunications Conference*, 1981.

[18] D. Cartier, "Limiter-discriminator detection performance of Manchester and NRZ coded FSK," *IEEE Transactions on Aerospace & Electronic Systems*, vol. 13, pp. 62–70, Jan 1977.

[19] C. Kwan, R. Simpson, and B. Batson, "Performance of biphase digital FM transmission," *IEEE Transactions on Communications*, vol. 25, p. 564, May 1977.

[20] I. Korn, "Comments on 'Limiter discriminator detection performance of Manchester and NRZ coded FSK,',"

[21] W. Tey and T. Tjhung, "Characteristics of Manchester-coded FSK," *IEEE Transactions on Communications*, vol. 27, pp. 209–216, 1979.

[22] H. Hartmann, "Spectrum of Manchester coded FSK," *IEEE Transactions on Communications*, pp. 1001–1004, October 1972.

[23] J. G. Proakis, *Digital Communications*. 1221 Avenue of the Americas, New York, NY, 10020: McGraw-Hill, 4th ed., 2001.

[24] G. K. Kaleh, "Simple coherent receivers for partial response continuous phase modulation," *IEEE Journal on Selected Arease in Communications*, vol. 7, pp. 1427–1436, December 1989.

[25] K. K. K. Murota and K. Hirade, "GMSK modulation for digital mobile radio telephony," *IEEE Transactions on Communications*, vol. 29, pp. 1044–1050, July 1981.

[26] K. Tsai and G. Lui, "Binary GMSK: Characteristics and performance," in *Proceedings of the International Telemetering Conference*, (Las Vegas, NV), 1999.

[27] A. V. Oppenheim, A. S. Willsky, and S. H. Nawab, *Signals & Systems*. Upper Saddle River, NJ, 07458: Prentice Hall, 2nd ed., 1997.

[28] J. B. Anderson, *Digital Transmission Engineering*. 445 Hoes Lane, P.O. Box 1331, Piscataway, NJ 08855-1331: IEEE Press, 1999.

[29] G. Lui and K. Tsai, "Viterbi and serial demodulators for pre-coded binary GMSK," in *Proceedings of the International Telemetering Conference*, (Las Vegas, NV), 1999.

[30] G. Colavolpe and R. Raheli, "Reduced-complexity detection and phase synchronization of CPM signals," *IEEE Transactions on Communications*, vol. 45, pp. 1070–1079, September 1997.

[31] A. Svensson, C.-E. Sundberg, and T. Aulin, "A class of reduced-complexity viterbi detectors for partial response continuous phase modulation," *IEEE Transactions on Communications*, vol. 32, pp. 1079–1087, October 1984.